JCI The Journal of Clinical Investigation

DNA repair deficiency sensitizes lung cancer cells to NAD$^+$ biosynthesis blockade

Mehdi Touat, … , Jean-Charles Soria, Sophie Postel-Vinay

J Clin Invest. 2018;128(4):1671-1687. https://doi.org/10.1172/JCI90277.

Research Article Oncology

Synthetic lethality is an efficient mechanism-based approach to selectively target DNA repair defects. Excision repair cross-complementation group 1 (ERCC1) deficiency is frequently found in non–small-cell lung cancer (NSCLC), making this DNA repair protein an attractive target for exploiting synthetic lethal approaches in the disease. Using unbiased proteomic and metabolic high-throughput profiling on a unique in-house–generated isogenic model of ERCC1 deficiency, we found marked metabolic rewiring of ERCC1-deficient populations, including decreased levels of the metabolite NAD$^+$ and reduced expression of the rate-limiting NAD$^+$ biosynthetic enzyme nicotinamide phosphoribosyltransferase (NAMPT). We also found reduced NAMPT expression in NSCLC samples with low levels of ERCC1. These metabolic alterations were a primary effect of ERCC1 deficiency, and caused selective exquisite sensitivity to small-molecule NAMPT inhibitors, both in vitro — ERCC1-deficient cells being approximately 1,000 times more sensitive than ERCC1-WT cells — and in vivo. Using transmission electronic microscopy and functional metabolic studies, we found that ERCC1-deficient cells harbor mitochondrial defects. We propose a model where NAD$^+$ acts as a regulator of ERCC1-deficient NSCLC cell fitness. These findings open therapeutic opportunities that exploit a yet-undescribed nuclear-mitochondrial synthetic lethal relationship in NSCLC models, and highlight the potential for targeting DNA repair/metabolic crosstalks for cancer therapy.

DNA repair deficiency sensitizes lung cancer cells to NAD+ biosynthesis blockade

Mehdi Touat,[1,2,3] Tony Sourisseau,[1] Nicolas Dorvault,[1,4] Roman M. Chabanon,[1,4] Marlène Garrido,[1,4] Daphné Morel,[1,4] Dragomir B. Krastev,[5] Ludovic Bigot,[1] Julien Adam,[1,6] Jessica R. Frankum,[5] Sylvère Durand,[7] Clement Pontoizeau,[8,9,10] Sylvie Souquère,[11] Mei-Shiue Kuo,[1] Sylvie Sauvaigo,[12] Faraz Mardakheh,[13] Alain Sarasin,[14] Ken A. Olaussen,[1,15] Luc Friboulet,[1] Frédéric Bouillaud,[16] Gérard Pierron,[11] Alan Ashworth,[17] Anne Lombès,[16] Christopher J. Lord,[5] Jean-Charles Soria,[1,2,15] and Sophie Postel-Vinay[1,2,4,5]

[1]Inserm U981, Gustave Roussy, Université Paris-Saclay, Villejuif, France. [2]Département d'Innovation Thérapeutique et d'Essais Précoces (DITEP), Gustave Roussy, Université Paris-Saclay, Villejuif, France. [3]Inserm U1127, CNRS UMR 7225, Sorbonne Universités, UPMC Université Paris 06 UMRS1127, Institut du Cerveau et de la Moelle Epiniere, ICM, Paris, France. [4]Inserm U981, ATIP-Avenir Team, Gustave Roussy, Université Paris-Saclay, Villejuif, France. [5]The CRUK Gene Function Laboratory and Breast Cancer Now Research Centre, The Institute of Cancer Research, London, United Kingdom. [6]Département de Biologie et Pathologies Médicales, and [7]Metabolomics Platform, Gustave Roussy, Université Paris-Saclay, Villejuif, France. [8]Centre de Référence des Maladies Héréditaires du Métabolisme, Hôpital Necker-Enfants Malades, Assistance Publique-Hôpitaux de Paris, Paris, France. [9]Service de Biochimie Métabolomique et Protéomique, Hôpital Necker-Enfants Malades, Assistance Publique–Hôpitaux de Paris, Paris, France. [10]Inserm U1163, Institut Imagine, Equipe "Génétique des Maladies Mitochondriales" and Paris Descartes University, Paris, France. [11]CNRS UMR-9196, Functional Organization of the Cell, Gustave Roussy, Université Paris-Saclay, Villejuif, France. [12]LXRepair, Grenoble, France. [13]Centre for Molecular Oncology, Barts Cancer Institute, Queen Mary University of London, London, United Kingdom. [14]CNRS UMR-8200, Laboratory of Genetic Stability and Oncogenesis, Gustave Roussy, Université Paris-Saclay, Villejuif, France. [15]Faculté de médecine Paris-Sud XI, Kremlin-Bicêtre. [16]Inserm U1016, CNRS UMR 8104, Institut Cochin, Université Paris-Descartes-Paris 5, Paris, France. [17]UCSF Helen Diller Family Comprehensive Cancer Center, UCSF, San Francisco, USA.

Synthetic lethality is an efficient mechanism-based approach to selectively target DNA repair defects. Excision repair cross-complementation group 1 (ERCC1) deficiency is frequently found in non–small-cell lung cancer (NSCLC), making this DNA repair protein an attractive target for exploiting synthetic lethal approaches in the disease. Using unbiased proteomic and metabolic high-throughput profiling on a unique in-house–generated isogenic model of ERCC1 deficiency, we found marked metabolic rewiring of ERCC1-deficient populations, including decreased levels of the metabolite NAD+ and reduced expression of the rate-limiting NAD+ biosynthetic enzyme nicotinamide phosphoribosyltransferase (NAMPT). We also found reduced NAMPT expression in NSCLC samples with low levels of ERCC1. These metabolic alterations were a primary effect of ERCC1 deficiency, and caused selective exquisite sensitivity to small-molecule NAMPT inhibitors, both in vitro — ERCC1-deficient cells being approximately 1,000 times more sensitive than ERCC1-WT cells — and in vivo. Using transmission electronic microscopy and functional metabolic studies, we found that ERCC1-deficient cells harbor mitochondrial defects. We propose a model where NAD+ acts as a regulator of ERCC1-deficient NSCLC cell fitness. These findings open therapeutic opportunities that exploit a yet-undescribed nuclear-mitochondrial synthetic lethal relationship in NSCLC models, and highlight the potential for targeting DNA repair/metabolic crosstalks for cancer therapy.

Introduction

Despite recent therapeutic advances, non–small-cell lung cancer (NSCLC) remains the leading cause of cancer death (1). Novel effective therapeutic approaches for this aggressive malignancy are therefore urgently required. The discovery of tumor-specific molecular alterations has revolutionized the development of targeted approaches for cancer. For example, genetic dependency effects such as oncogene addiction and synthetic lethal interactions offer the potential to selectively target driver mutations or genetic deficiencies in cancer.

Excision repair cross-complementation group 1 (ERCC1), a key player of the nucleotide excision repair (NER) and interstrand crosslink repair (ICL-R) pathways, is the most frequent deficient DNA repair protein in NSCLC (reviewed in ref. 2). ERCC1 deficiency correlates with sensitivity to agents that stall DNA replication forks, such as platinum salts and PARP inhibitors (3–5). However, drug resistance and/or cumulative toxicities ultimately occur, limiting drug efficacy. Additional therapeutic approaches targeting ERCC1-deficient cancers are thus needed.

Many of the synthetic lethal approaches for cancer treatment to date have focused on interactions within DNA repair pathways, associating inhibition of DNA repair enzymes to defects in DNA repair–related tumor suppressor genes, for example, poly(ADP-ribose) polymerase 1 (PARP1) inhibition in *BRCA1*- or *BRCA2*-mutant tumors (reviewed in ref. 6). Far less emphasis has been placed on inhibition of non–DNA repair processes in tumor cells with preexisting DNA repair defects. Previous studies revealed that DNA damage response can directly or indirectly impact cellular metabolism, and that aging and defects in DNA repair machin-

Authorship note: JCS and SPV are co-senior authors.
Conflict of interest: The authors have declared that no conflict of interest exists.
Submitted: August 23, 2016; **Accepted:** February 1, 2018.
Reference information: *J Clin Invest*. 2018;128(4):1671–1687.
https://doi.org/10.1172/JCI90277.

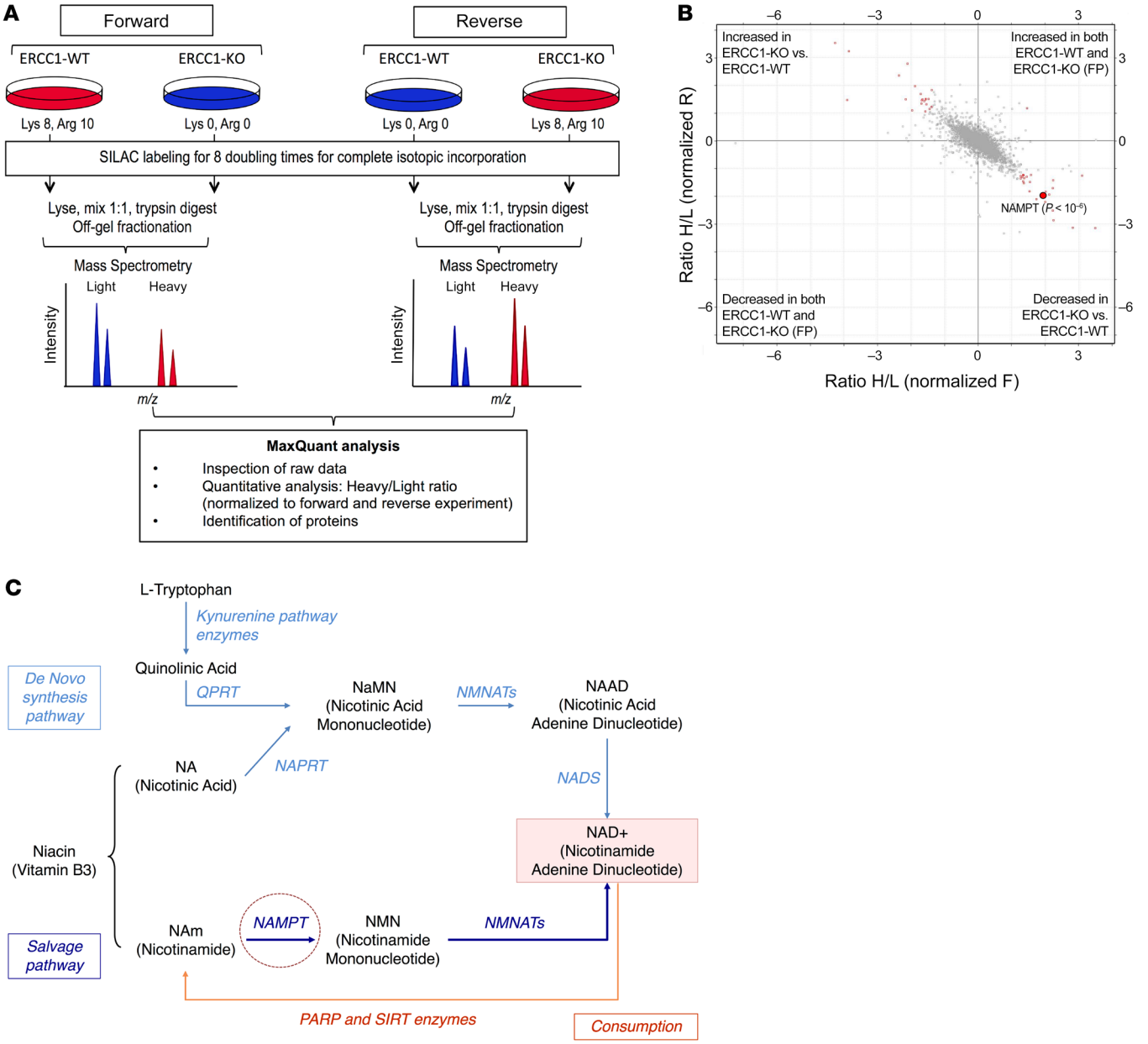

Figure 1. SILAC-based proteomic analysis identifies NAMPT decrease as a potentially targetable node in ERCC1-deficient clones. (**A**) Experimental workflow for quantitative proteomic analysis using SILAC. Two independent experiments in the ERCC1-WT and ERCC1-KO cell lines from the A549 model with inverted labeling of the cell lines (forward and reverse experiments) were set up and run in parallel in order to limit the number of false-positive hits by having an internal control (n = 2 independent samples for each model). Protein lysates were mixed in a 1:1 proportion between the heavy- and light-labeled cells. After protein digestion and off-gel fractionation, fractions were analyzed by LC-MS/MS, and data analysis was performed by MaxQuant. (**B**) Scatter plot of the ratio of heavy over light amino acids normalized to the reverse (R) or forward (F) experiment, following a log2 normalization. Hits reaching significance (Benjamini-Hochberg adjusted P value < 0.05) in both experiments are depicted in red. FP, false-positive. (**C**) Canonical NAD⁺ biosynthetic pathways. In humans, most NAD⁺ is synthesized from nicotinamide (NAm) through the salvage (recycling) pathway. NAMPT (NAm phosphoribosyltransferase) catalyzes the rate-limiting step in this pathway. Sirtuins (SIRTs) and poly(ADP-ribose) polymerase (PARPs) enzymes catalyze reactions that consume NAD⁺. The reaction scheme is based on the Biocyc pathway map for homo sapiens NAD⁺ biosynthesis (http://biocyc.org/), and adapted from Kim et al (15). NAPRT, nicotinic acid phosphoribosyltransferase; QPRT, quinolinic acid phosphoribosyltransferase; NMNATs, NMN adenylyltransferases; NADS, NAD⁺ synthetase.

ery could contribute to alterations in mitochondrial function and energy metabolism (7–11). Mouse models of xeroderma pigmentosum group A (XPA) and Cockayne syndrome group B (CSB) display aberrant activation of the DNA repair enzymes PARPs with concomitant depletion of nicotinamide adenine dinucleotide (NAD⁺) and mitochondrial dysfunction, which can be partly rescued by supplementation with NAD⁺ precursors (8, 9). NAD⁺ acts as rate-limiting cofactor for the DNA repair enzyme PARPs (12). PARP1, whose activation catabolizes a significant amount of NAD⁺ (7, 12), is the most abundant nuclear protein of the PARP family and serves as sensor to DNA damage (6). Deciphering and exploiting interactions between these 2 hallmarks of cancer — namely DNA

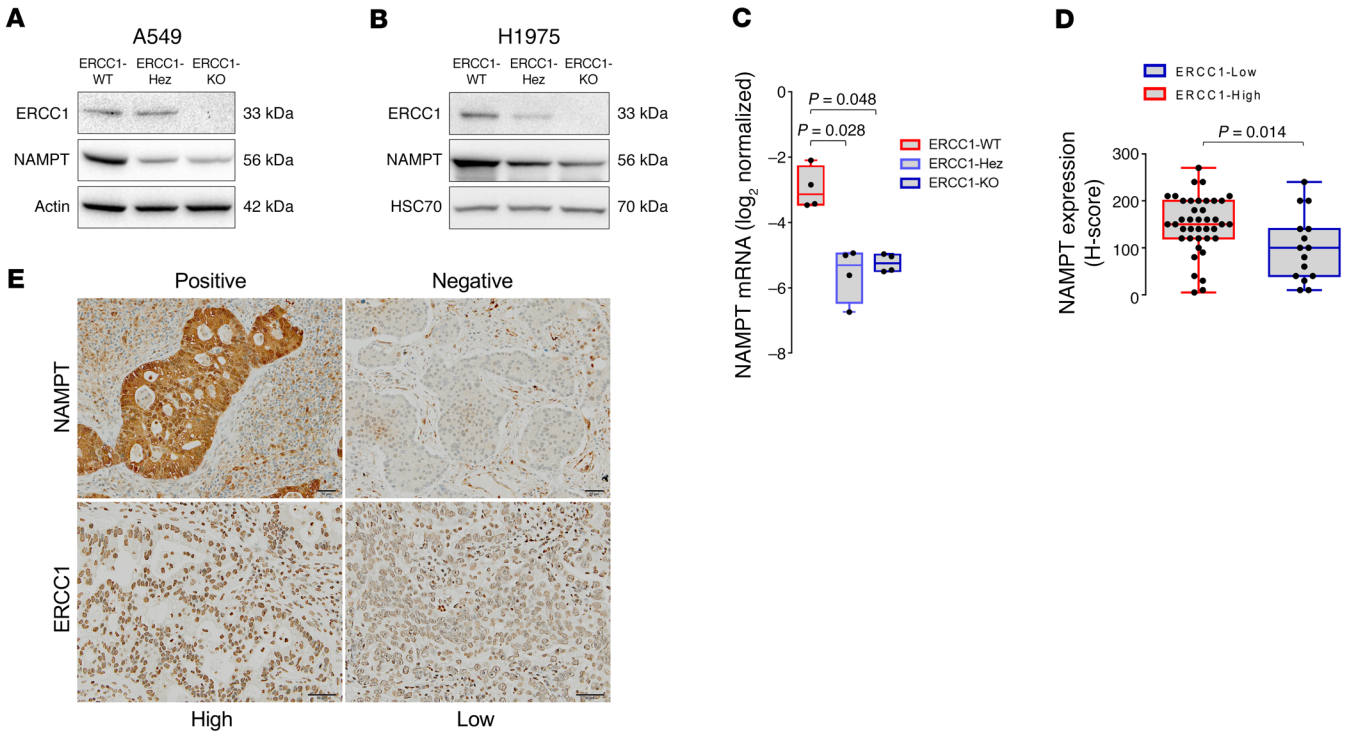

Figure 2. ERCC1 expression correlates with NAMPT expression in human adenocarcinoma cell lines and patient samples. (**A** and **B**) Representative Western blot of NAMPT and ERCC1 protein expression in the ERCC1-deficient isogenic models derived from the A549 (**A**) and H1975 (**B**) NSCLC cell lines. Data were replicated in 3 independent experiments. (**C**) NAMPT mRNA levels in ERCC1-WT, ERCC1-Hez, and ERCC1-KO cell lines from the A549 model. Data are box plots of NAMPT mRNA levels (± minimal and maximal values) with $n = 4$ independent experiments for each model. Statistical analyses are indicated (Kruskal-Wallis 1-way ANOVA adjusted using Dunn's multiple comparison test). (**D**) ERCC1 and NAMPT immunohistochemical stainings in human adenocarcinoma samples. Data are box plots (± minimal and maximal values) showing NAMPT protein expression according to ERCC1 expression in $n = 55$ tumor samples. Statistical analyses are indicated (Mann-Whitney *U* test). (**E**) Representative images of ERCC1 and NAMPT immunohistochemical stainings in human tumor samples. Scale bar: 50 μm.

damage response and dysregulation of cellular energetics — could therefore unravel mechanism-based therapeutic opportunities for targeting DNA repair defects in human malignancies.

We hypothesized that ERCC1 deficiency resulted in metabolic reprogramming of cancer cells that in turn generated specific metabolic vulnerabilities. To explore that hypothesis, we used an unbiased large-scale comparative approach based on proteomic and metabolic profiling of isogenic NSCLC models of ERCC1 deficiency. This allowed us to identify striking metabolic differences between ERCC1-proficient and ERCC1-deficient NSCLC cells. Among them, decreased NAD^+ and mitochondrial defects were associated with a profound selective sensitivity to NAD^+ depletion induced by nicotinamide mononucleotide phosphoribosyl-transferase (NAMPT) inhibition in ERCC1-deficient cells. Data presented here unveil promising synthetic lethal approaches based on metabolic targeting of ERCC1-deficient NSCLC populations.

Results

A proteomic screen identifies NAMPT as significantly decreased in ERCC1-deficient NSCLC cells. In order to understand proteomic differences between ERCC1-proficient and ERCC1-deficient cells, we performed a high-throughput SILAC (stable isotope labeling by amino acids in cell culture) analysis. To maximize the potential for identifying ERCC1-selective effects, we used our in-house–generated panel of ERCC1-isogenic cell lines, where *ERCC1* had been inactivated by zinc finger gene targeting (5, 13). This panel, derived from the A549 NSCLC cell line, includes 8 cell populations: 1 parental ERCC1-WT, 1 ERCC1-heterozygous (Hez), 2 ERCC1-deficient (KO1 and KO2), and 4 "rescue" ERCC1-KO in which one of the 4 ERCC1 isoforms has been stably reintroduced (isoforms 201, 202, 203, or 204, respectively). As previously reported, this model is representative of the clinical and biological characteristics associated with ERCC1 deficiency (4, 5, 13). The ERCC1-proficient parental cell line and 1 ERCC1-deficient clone were grown in culture media only differing by isotopic amino acids (aa) (Figure 1A): the "light" culture contained unlabeled aa (Lys 0, Arg 0) whereas the "heavy" culture contained isotope-labeled aa (Lys 8, Arg 10). After 8 doubling times, proteins were extracted, digested, off-gel fractionated, and analyzed using liquid chromatography-tandem mass spectrometry (LC-MS/MS). A forward and a reverse experiment in which isotope labeling was inverted between cell lines were performed in parallel in order to minimize false-positive results. This approach identified 45 hits (out of 5,051 known proteins), which were significantly differentially expressed between the ERCC1-WT and the ERCC1-KO cells (Figure 1B). Among these hits, 2 proteins were involved in the NAD^+ biosynthesis pathway: NAMPT and NNMT (nicotinamide N-methyltransferase) (2- and 3.1-fold decrease in ERCC1-KO cells respectively, $P < 10^{-6}$) (Figure 1B). Three subunits of complex IV (cytochrome c oxidase)

of the mitochondrial respiratory chain (COX4I1, COX5B, and COX6C) were also significantly decreased in ERCC1-KO populations (1.3-, 2.1-, and 2.5-fold, respectively, $P < 0.0001$).

NAMPT catalyzes the rate-limiting step of the NAD^+ biosynthesis salvage pathway (Figure 1C), thereby playing a crucial role in the maintenance of intracellular NAD^+, an essential cofactor involved in several cellular reactions, including cellular energetics and DNA repair (14, 15). Growing evidence indicates that NAMPT exerts oncogenic activity in the context of cancer. Several NAMPT inhibitors have already been evaluated in early phase trials (16), with others being currently developed (17). NAMPT therefore appeared to be a targetable node in ERCC1-defective tumors, and we decided to further focus on this target.

Decreased NAMPT expression is found in several ERCC1-deficient NSCLC models and in immunohistochemical study of lung adenocarcinomas. Because high-throughput experiments are prone to false positives, we validated the observed NAMPT decrease by Western blot in the A549 isogenic model (Figure 2A). We then sought to extend this finding to an alternative ERCC1 isogenic model created using the same gene targeting procedure (ZNFs) in the H1975 NSCLC cell line (Figure 2B), which harbors a different genetic background (18). Consistent with our observations in the A549 model, NAMPT levels were significantly decreased in the ERCC1-Hez and ERCC1-KO cells of the H1975 model. The observation of decreased NAMPT in the ERCC1-Hez populations suggested a haploinsufficiency phenomenon. We then explored whether the decrease in NAMPT protein levels in ERCC1-deficient cells was a consequence of a transcriptional (mRNA) or posttranscriptional regulation. Real-time reverse transcription PCR (RT-qPCR) performed on mRNA extracts and evaluation of bortezomib (a proteasome inhibitor) on NAMPT protein levels in the A549 isogenic model revealed that NAMPT decrease was controlled at the mRNA level (Figure 2C and Supplemental Figure 1; supplemental material available online with this article; https://doi.org/10.1172/JCI90277DS1).

To address the clinical relevance of the NAMPT decrease, we assessed ERCC1 and NAMPT expression by immunohistochemistry on a series of 55 resected human lung adenocarcinoma samples (Figure 2, D and E and Supplemental Figure 2). The median NAMPT staining H-score was 150 (SD = 72) for the ERCC1-high samples (n = 40), whereas it was 100 (SD = 60) for the ERCC1-low samples. Although some degree of overlap was observed in both populations, this difference was statistically significant ($P = 0.014$; Figure 2D).

Collectively, these results show that in NSCLC cellular models as well as in human adenocarcinoma samples, ERCC1 deficiency associates with a significant decrease in NAMPT, which is most likely controlled at the transcriptional level.

Decreased NAMPT in ERCC1-deficient NSCLC cells leads to profound synthetic lethal sensitivity to NAMPT inhibition. In humans, most NAD^+ is produced from the nicotinamide salvage pathway (Figure 1C) (14). As NAMPT is the rate-limiting enzyme of the salvage pathway, its inhibition represents a potent way to efficiently lower cellular NAD^+ levels. We hypothesized that inhibiting NAMPT in ERCC1-deficient cells, and consequently further reducing NAD^+ levels, might impact cellular fitness.

Exposure of tumor cells to FK866 (Figure 3A), a highly specific noncompetitive inhibitor of NAMPT, revealed dramatic and profound sensitivity of ERCC1-KO cells (Figure 3, B–D). FK866 IC_{50} was 100 times lower in ERCC1-KO cells than in ERCC1-proficient ones in short-term assays (Figure 3B), and was 1,000 times lower in long-term colony formation assays (Figure 3, C and D). Interestingly, ERCC1-Hez cells were as sensitive to FK866 as ERCC1-KO cells, again suggesting haploinsufficiency (Figure 3, B–D). The study of cell death mechanisms showed PARP1 cleavage and increased annexin V–positive populations on FK866 exposure in ERCC1-deficient cells, without LC3 cleavage, suggesting that apoptosis was responsible for cell death (Figure 3, E and F, and Supplemental Figure 3).

Synthetic lethal sensitivity to NAMPT inhibition is a primary effect of ERCC1 deficiency. In order to confirm the specificity of the observed effect, we used several alternative models to revalidate our findings: (a) the 4 ERCC1-KO cell lines in which each ERCC1 isoform had been stably reintroduced, (b) the alternative isogenic cell line model derived from the H1975 cell line, and (c) a nonisogenic panel of NSCLC cell lines.

Only ERCC1 isoform 202 has been shown to be responsible for ERCC1 DNA repair activity as well as sensitivity to platinum salts and PARP inhibitors (5, 13). The role and functionality of the 3 other isoforms are still unknown. NAMPT protein expression was only restored in the ERCC1-KO cell line in which isoform 202 had been stably reintroduced (Figure 4A), and remained unchanged upon reintroduction of the other isoforms. Consistently, isoform 202 was the only one able to restore FK866 resistance in rescue experiments (Figure 4B). Despite having a different genetic background, the alternative H1975 isogenic models of ERCC1 deficiency displayed a similar sensitivity to FK866 as that of the A549 models (Figure 4C). Interestingly, both ERCC1-KO and ERCC1-Hez cell lines were again profoundly more sensitive to FK866 than their ERCC1-proficient counterparts, suggesting a haploinsufficiency phenomenon that is not observed with cisplatin (Supplemental Figure 4A). To extend our findings, we assessed sensitivity to FK866 in a nonisogenic panel that included 3 additional NSCLC cell lines genetically different from A549 and H1975 cells. NSCLC cells expressing lower ERCC1 protein levels were more sensitive to FK866 than the ones expressing higher ERCC1 levels (Supplemental Figure 4, B and C).

Altogether, the ability of ERCC1 isoform 202 to rescue sensitivity to FK866 and the FK866 selectivity toward ERCC1-deficient populations in multiple independent ERCC1-deficient models support the notion that the sensitivity to NAMPT inhibition is directly related to ERCC1 deficiency.

The ERCC1-NAMPT synthetic lethal relationship is related to the disruption of the NAD^+ salvage pathway. As small molecule inhibitors have potential off-target effects, we assessed ERCC1-deficient cells' sensitivity to GNE-617, an alternative small-molecule NAMPT inhibitor (Figure 3A). This latter compound showed similar selectivity with regards to ERCC1-deficient cells (Figure 4D), supporting an on-target and class effect.

We then evaluated the impact of the addition of nicotinamide mononucleotide (NMN, the direct product of NAMPT enzymatic activity) (Figure 1C) on NAMPT inhibitor sensitivity. Addition of NMN to the culture media reversed the toxicity of the 2 small-molecule NAMPT inhibitors in both isogenic models, confirming their on-target effect (Figure 4, E and F, and Supplemental Figure 4D). Further, silencing of NAMPT by siRNA showed selective toxicity toward ERCC1-deficient populations (Figure 4, G and H), thereby reinforcing the on-target characteristic of the observed effect.

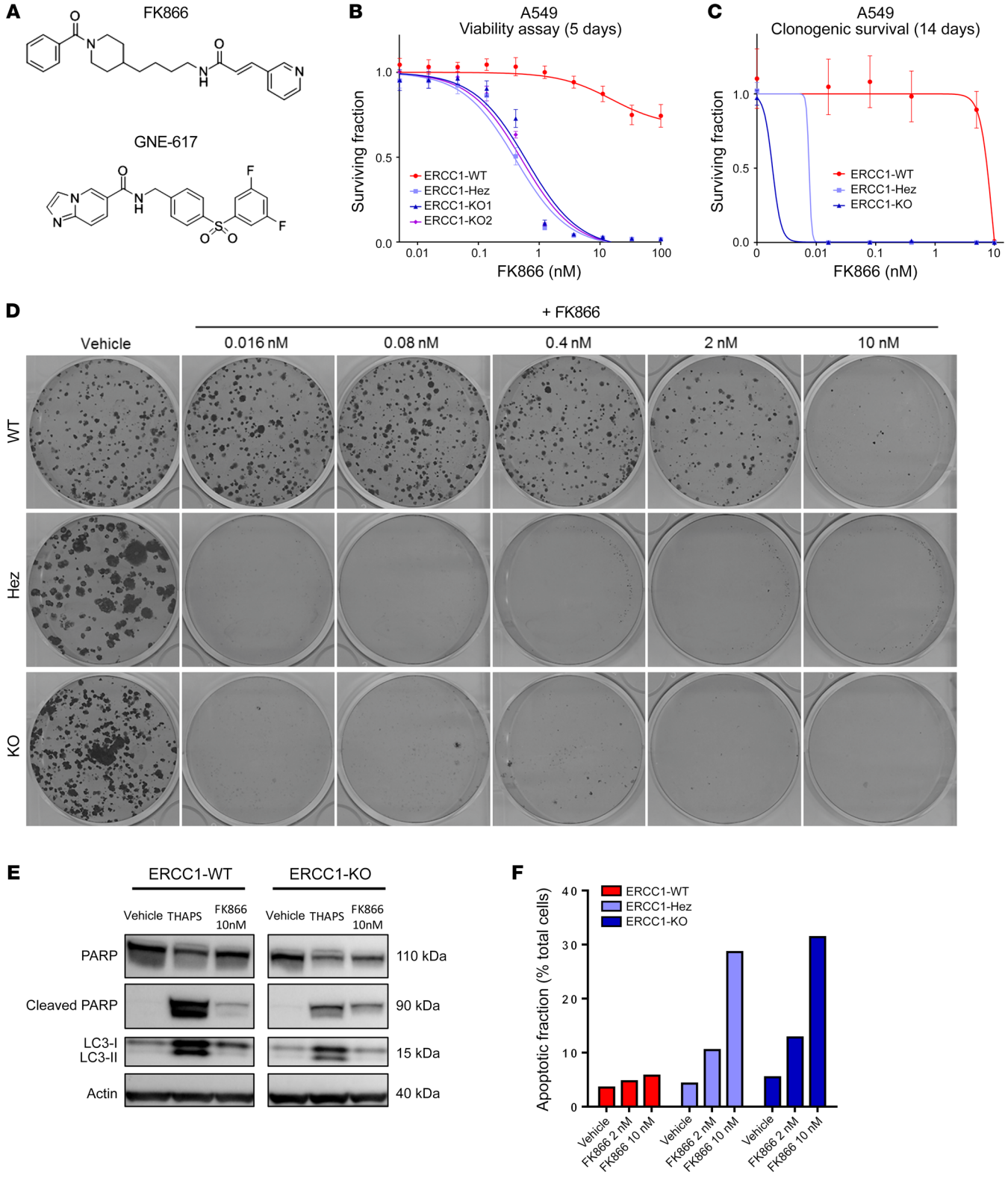

Figure 3. NAMPT decrease in ERCC1-deficient clones leads to exquisite sensitivity to NAMPT inhibitors. (**A**) Chemical structures of NAMPT inhibitors FK866 and GNE-617. (**B** and **C**) Survival curves of the A549 ERCC1 isogenic model on FK866 exposure in short-term assay (**B**) and long-term colony formation assay (**C**). Data are mean surviving fractions ± SD from 1 of 3 independent experiments. (**D**) Pictures of the colony formation assay in the A549 ERCC1 isogenic model after 14 days of treatment with vehicle or FK866. (**E**) Representative Western blot of PARP and LC3 protein expression in A549 ERCC1-proficient and ERCC1-deficient cells treated with vehicle or FK866. Thapsigargin (THAPS) was used as positive control for apoptosis and induction of autophagy. Data are from 1 experiment. (**F**) Fraction of annexin V–positive (both 7-AAD–negative or 7-AAD–positive) cells determined by flow cytometry analysis after 5 days of exposure with FK866 in A549 ERCC1-proficient and ERCC1-deficient cells. Data are from 1 experiment.

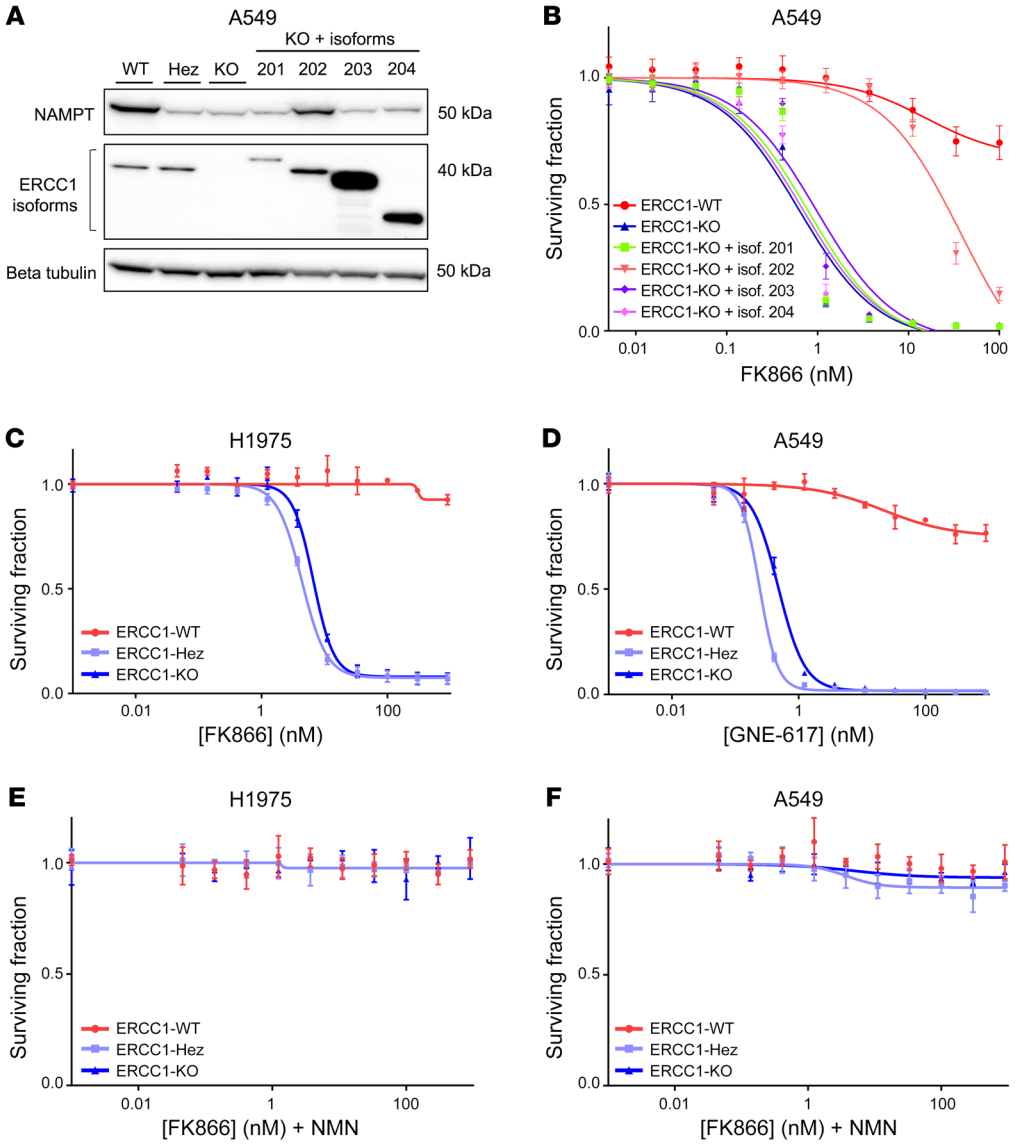

Figure 4. Exquisite sensitivity to NAMPT inhibition is a primary effect of ERCC1 deficiency. (**A**) Representative Western blot of NAMPT and ERCC1 protein expression and (**B**) survival experiment on FK866 exposure according to the reintroduction of the 4 alternative ERCC1 isoforms. (**C**) Survival experiment on FK866 exposure of the H1975 ERCC1-isogenic model. (**D**) Survival experiment on GNE-617 exposure of the A549 ERCC1-isogenic model. (**E** and **F**) Rescue of FK866 toxicity by the administration of nicotinamide mononucleotide (NMN) 100 μM in the H1975 (**E**) and A549 (**F**) ERCC1-isogenic models. Data for **B**–**F** are mean surviving fraction ± SD from 1 experiment. (**G**) Cell viability after acute NAMPT silencing by siRNA in A549 ERCC1-proficient and ERCC1-deficient cells. Toxicity of PLK1 silencing by siRNA was used as a positive control for cell death induction. Data are mean viability ± SD from 1 representative experiment. Statistical analyses are indicated (Mann-Whitney *U* test corrected for multiple comparisons). NS indicates no statistically significant difference. (**H**) Representative Western blot of NAMPT and ERCC1 protein expression after NAMPT silencing by siRNA in A549 ERCC1-proficient and ERCC1-deficient cells. For **A**–**H**, data were replicated in at least 3 independent experiments.

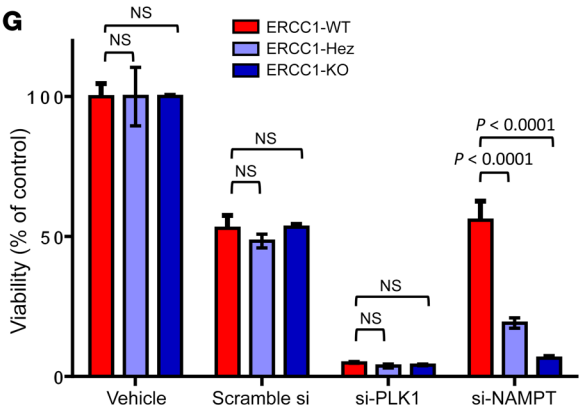

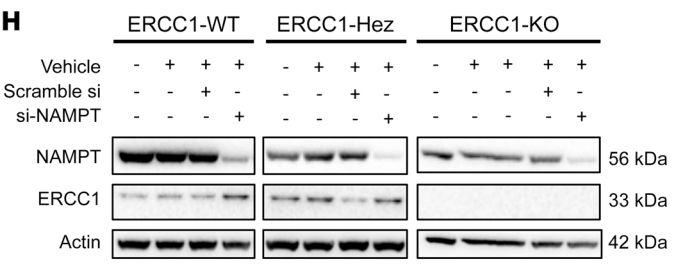

Together, these data support that the synthetic lethal relationship between ERCC1 deficiency and NAMPT results from the concomitant disruption of ERCC1-dependent functions and the NAD^+ recycling pathway, and indicate that minimal residual NAMPT activity is essential for survival of ERCC1-deficient NSCLC cells.

NAMPT inhibition is exquisitely toxic to ERCC1-KO cells in vivo. To address the in vivo relevance of NAMPT inhibition, we implanted equal amounts of either ERCC1-WT or ERCC1-KO cells into 6-week-old athymic nude (nu/nu) mice. Once tumors reached a minimal volume of 100 mm^3, mice were randomly allocated

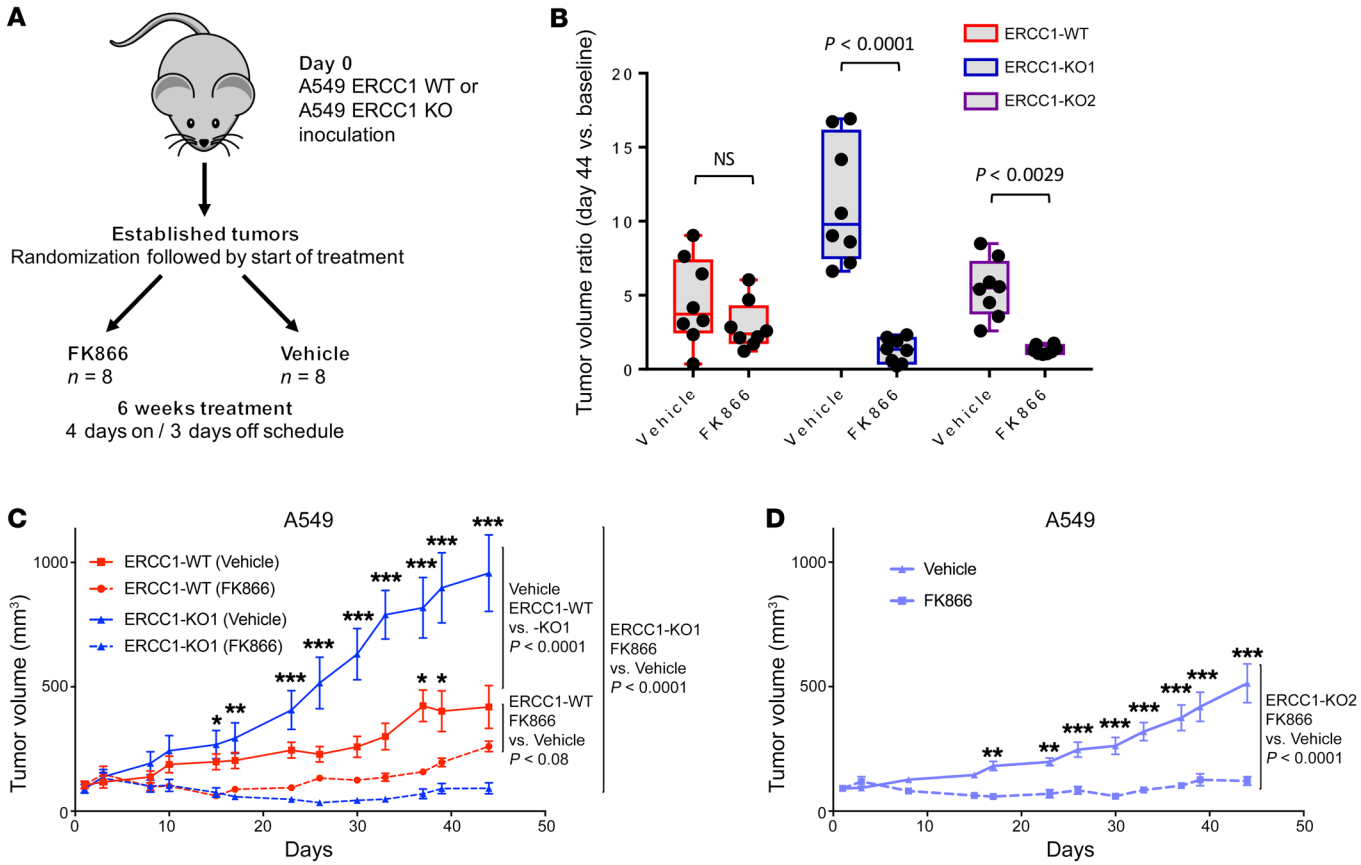

Figure 5. NAMPT inhibition is synthetic lethal with ERCC1 deficiency in in vivo models of NSCLC. (**A**) Experimental workflow for the in vivo experiments. Treatment was initiated when tumors reached a volume of 100 mm^3. Tumor-bearing mice (n = 8 per group) were randomized to receive 30 mg/kg/day FK866 or vehicle for 6 weeks following a 4 days on, 3 days off schedule. (**B**) Changes in tumor volume after 44 days of treatment with FK866 in ERCC1-proficient and ERCC1-deficient tumors in nude mice. Data are mean tumor volume ± SD (n = 8 mice per group). Statistical analyses are indicated (2-way ANOVA adjusted for multiple comparisons using Bonferroni's post hoc test). (**C** and **D**) Tumor growth on FK866 treatment in the A549 ERCC1-WT and ERCC1-KO1 models (**C**), and in the ERCC1-KO2 model (**D**). Data represent mean tumor volume ± SEM (n = 8 mice per group). Statistical analyses are indicated (2-way ANOVA adjusted for multiple comparisons using Bonferroni's post hoc test). *P < 0.05, **P < 0.01, ***P < 0.0001.

to FK866 or vehicle treatment (Figure 5A). An FK866 administration schedule (i.p. injection twice a day, 4 days on, 3 days off) was selected based on previous efficacy-tolerability studies (19). Although FK866 delayed tumor growth in all populations, only ERCC1-KO models displayed a significant difference in tumor volumes between the FK866 and vehicle groups (Figure 5, B–D). This effect was much more profound and prolonged in ERCC1-KO xenografts (Figure 5, C and D) than in ERCC1-WT xenografts, with some tumors being not palpable after 20 to 48 days of treatment. Mice weights were similar in all experimental arms over the whole treatment duration, confirming adequate tolerability of this dosing schedule (Supplemental Figure 5, A–C). These results demonstrate that NAMPT inhibition causes tumor shrinkage and decreased growth of established ERCC1-deficient xenografts in vivo.

ERCC1-deficient cells present a characteristic metabolic profile, including alterations in the TCA cycle and NAD⁺ biosynthesis pathway. The initial SILAC screen showed decreased protein expression of NAMPT, NNMT, and 3 subunits of the mitochondrial respiratory complex IV, which led us to hypothesize altered NAD^+ biosynthesis and mitochondrial dysfunction in ERCC1-deficient cells. In order to investigate these metabolic disturbances, we performed a large-scale metabolic profiling of 2 ERCC1-KO clones, the ERCC1-Hez cell line and the ERCC1-WT cell line from our A549 isogenic model, using LC-MS/MS, gas chromatography–tandem mass spectrometry (GC-MS/MS), and LC–quadrupole time-of-flight (LC-QTOF). Combined analysis of these 3 assays (see Methods) resulted in a final data set of 1,947 metabolites defined by high-resolution m/z identification, 159 of which were kept for further analysis. These 159 metabolites had previously been validated by the metabolomics platform (annotated panel) and were annotated as level 1 according to the recommendations of the Metabolomics Society.

Unsupervised clustering of the 159 annotated metabolites showed that all ERCC1-deficient cell lines clustered together and according to their ERCC1 status, away from their ERCC1-proficient counterparts (Figure 6A). Of note, this unsupervised clustering based on metabolites recapitulated the clustering based on ERCC1 expression, thereby supporting a link between genetic and metabolic abnormalities. The heterozygous cell line metabolic profile was closer to that of the ERCC1-KO clones than it was to that of the ERCC1-WT parental cell line, in agreement with the haploinsufficiency previously observed for NAMPT expression

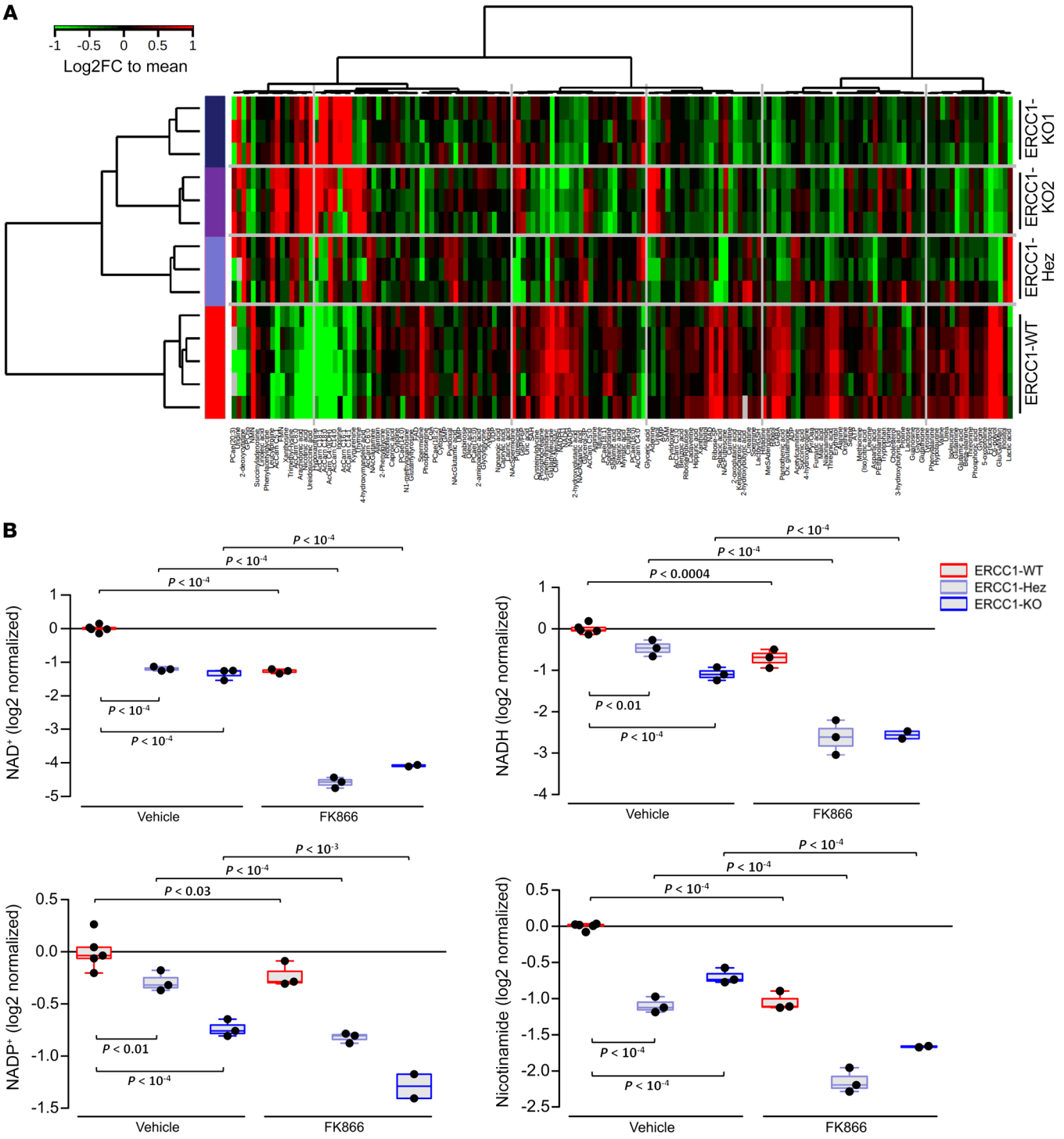

Figure 6. ERCC1-deficient cells present a characteristic metabolic profile with alterations in the NAD⁺ biosynthesis pathway. (**A**) Heatmap depicting relative abundance of 159 metabolites (annotation level 1, see Methods) determined by metabolomic profiling in the ERCC1-WT (n = 5 independent samples), ERCC1-Hez (n = 3), and ERCC1-KO (n = 3) cell lines from the A549 model. Samples (rows) and metabolites (columns) were reordered by hierarchical clustering using the Ward algorithm on their respective Euclidean distance matrices. (**B**) Box plots showing the relative abundance of central metabolites of the NAD⁺ pathway (NAD⁺, NADH, NADP, and nicotinamide) across the ERCC1-WT (n = 5 independent samples), ERCC1-Hez (n = 3), and ERCC1-KO (n = 3) cell lines with and without treatment by FK866. Data were centered on the ERCC1-WT vehicle group for comparative purposes. All statistical analyses and data representation were performed on preprocessed, log2-transformed and imputed data and reported as such without back transformation. Moderated statistics were used for differential analysis. Levels of significance were denoted as adjusted Benjamini-Hochberg P values to control the FDR.

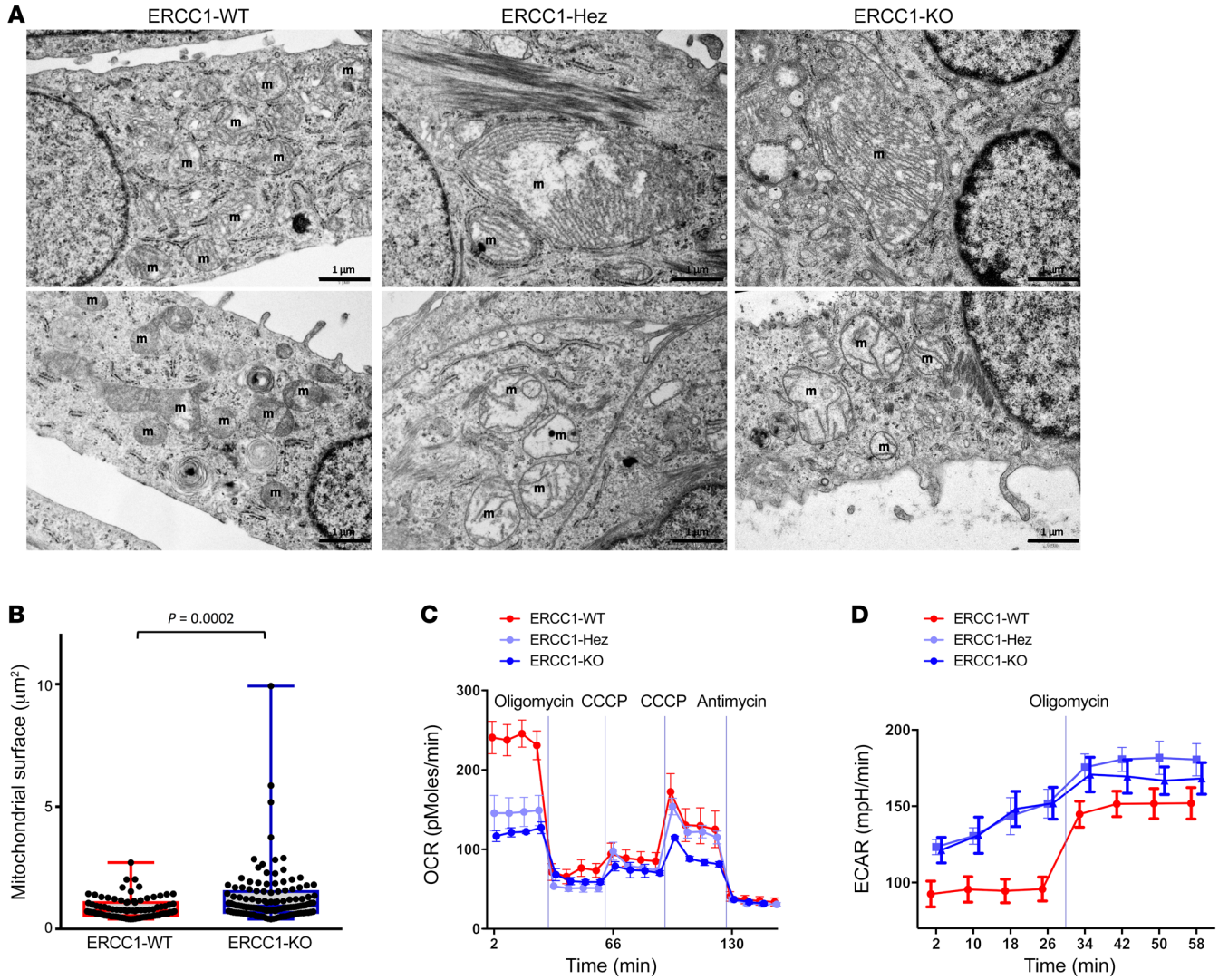

Figure 7. ERCC1-deficient cells present an abnormal mitochondrial structure associated with decreased respiratory capacity and increased glycolysis. (**A**) Representative transmission electron microscopy (TEM) pictures of the A549 ERCC1-WT, ERCC1-Hez, and ERCC1-KO cell lines. m, mitochondria. Scale bars: 1 μm. (**B**) Measurements of mitochondrial area using TEM in A549 ERCC1-deficient and ERCC1-proficient cells. Data are box plots (± minimal and maximal values) from n = 87–122 mitochondria per group. Statistical analyses are indicated (Mann-Whitney U test). (**C** and **D**) OCR and ECAR of intact A549 ERCC1-WT, ERCC1-Hez, and ERCC1-KO cells measured in real time with the Seahorse XF96 analyzer. Indices of glycolysis and mitochondrial function were measured after sequential injections of oligomycin (1 μg/ml final), CCCP (first 0.25 μM then 0.50 μM), and antimycin A (1 μg/ml). Data are mean ± SD from 1 experiment. OCR, oxygen consumption rate; ECAR, extracellular acidification rate; CCCP, carbonyl cyanide 3-chlorophenylhydrazone. For **A**–**D**, data were replicated in 3 independent experiments.

and NAMPT inhibitor sensitivity (Figure 2, A and B; Figure 3, B and C; Figure 4; Supplemental Figure 3; and Supplemental Figure 4). This metabolic profiling revealed a significantly different expression of several metabolites from the NAD^+ biosynthesis pathway (Figure 6B). NAD^+, NADH, $NADP^+$, NADPH, nicotinamide, and NMN were significantly diminished (1.5- to 2.5-fold) in ERCC1-KO models as compared with ERCC1-WT cells (Figure 6, A and B). This was accompanied by changes in several metabolites from the TCA cycle: citrate/isocitrate and 2-oxoglutarate were significantly decreased (all $P < 0.05$), whereas succinate was significantly increased in ERCC1-deficient cell lines ($P < 0.05$) (Supplemental Figure 6A). Assessment of the succinate dehydrogenase inhibition did not alter fumarate and succinate levels, thereby suggesting that the underlying mechanism might not be a flow reversal from fumarate to succinate in the TCA (Supplemental Figure 6B). Several fatty acid–derived acylcarnitines were significantly increased in ERCC1-deficient cells (all $P < 0.05$) (Supplemental Figure 6C), in a pattern encountered when beta-oxidation is disrupted. Combined alteration of TCA and beta-oxidation are expected consequences of defective oxidative phosphorylation. Altogether, the metabolic data supported that ERCC1 deficiency was associated with a significant metabolic rewiring affecting NAD^+ biosynthesis and oxidative phosphorylation in NSCLC cells.

FK866 exposure dramatically exacerbates baseline metabolic differences between ERCC1-proficient and ERCC1-deficient models. In order to assess whether the FK866 selective effect on ERCC1-deficient models was driven by metabolic changes, we investigated the effects of FK866 at a nonlethal dose on large-scale metabolic

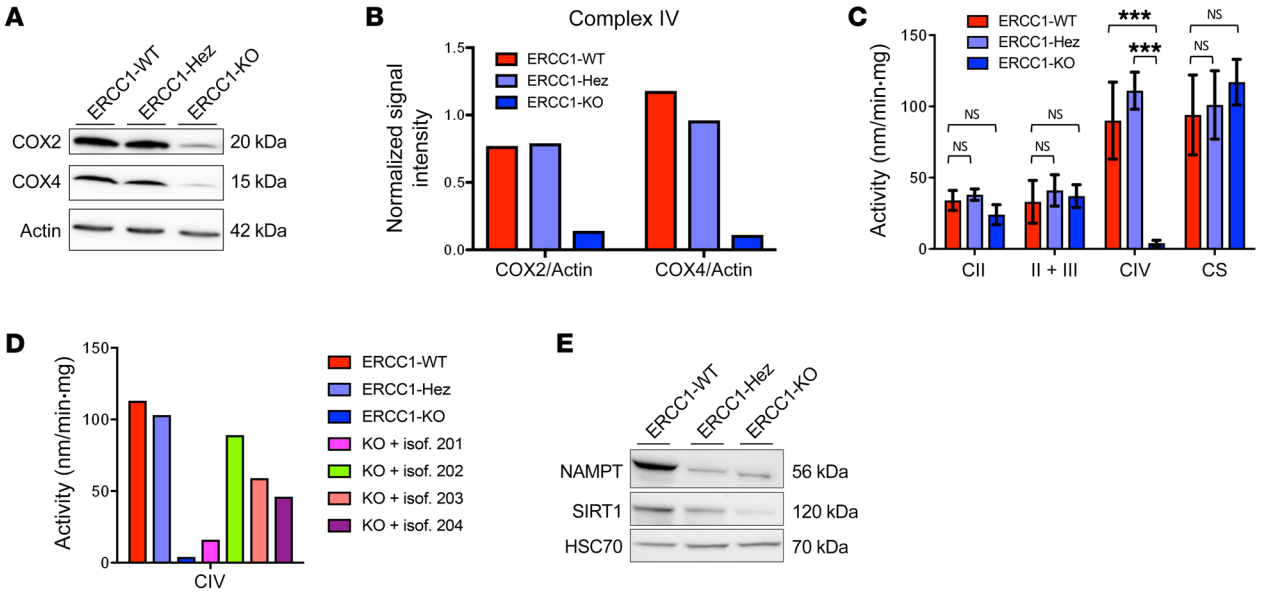

Figure 8. ERCC1-KO cells have a decreased mitochondrial complex IV activity associated with decreased SIRT1 protein expression. Representative Western blot (**A**) and quantification (**B**) of COX2 and COX4 protein expression in A549 ERCC1-proficient and ERCC1-deficient cell lines. Data were replicated in 3 independent experiments. (**C**) Enzymatic activities of mitochondrial complexes measured using respiratory chain spectrophotometric assay in A549 ERCC1-proficient and ERCC1-deficient cell lines (n = 3 independent samples per group). Data are mean enzymatic activity ± SD. Statistical analyses are indicated (2-way ANOVA adjusted using Tukey's multiple comparison test). NS indicates no statistically significant difference. ***$P < 0.0001$. (**D**) Enzymatic activity of mitochondrial complex IV in A549 ERCC1-proficient and ERCC1-deficient models in which each ERCC1 isoform has been stably reintroduced. Data are from 1 experiment. (**E**) Western blot of NAMPT and SIRT1 protein expression in A549 ERCC1-WT, ERCC1-Hez, and ERCC1-KO cells. Data are from 1 experiment.

profiling. After 24 hours of drug exposure, cells were lysed and metabolites were extracted for GC-MS/MS and LC-MS/MS + LC-QTOF analyses. As expected, FK866 exposure caused a profound decrease in NAD^+, NADH, NADP, NADPH, and nicotinamide levels in all cell lines (Figure 6B). This effect was strikingly more marked in ERCC1-deficient populations (ERCC1-KO and ERCC1-Hez) than in their ERCC1-proficient counterparts, with metabolites from the NAD^+ biosynthesis pathway becoming among the most differentially expressed on FK866 exposure (Supplemental Figure 7A). In ERCC1-deficient cells exposed to FK866, the NAD^+ level was down to an 8-fold decrease, whereas only a 2-fold decrease was observed in the ERCC1-WT population (Figure 6B). Disturbances among intermediates of the TCA cycle (isocitrate, 2-oxoglutaric acid, succinic acid, and fumaric acid) were exclusively observed in the ERCC1-deficient cells (Supplemental Figure 6A). ATP/ADP (adenosine diphosphate) and ADP/AMP (adenosine monophosphate) ratios, 2 major sensors of energetic equilibrium, were markedly decreased in ERCC1-Hez and ERCC1-KO cells (Supplemental Figure 7B), whereas ATP levels were conserved, suggesting the activation of alternative reactions to maintain cellular ATP homeostasis. These results show that FK866 treatment exacerbates NAD^+ depletion as well as its associated consequences on TCA and bioenergetics.

ERCC1-deficient cells display abnormal mitochondrial structure, decreased respiratory capacity, and increased glycolysis, but not elevated ROS levels. Alterations found in TCA cycle and beta-oxidation, 2 major mitochondrial pathways, led us to analyze mitochondrial ultrastructure by electron microscopy. ERCC1-Hez and ERCC1-KO cells displayed abnormal mitochondrial ultrastructure and associated mitochondrial swelling (a mark of mitochondrial dysfunction, ref. 20), increased mitochondrial area (mean area 0.86 μm² in the ERCC1-WT cells versus 1.28 μm² in the ERCC1-KO cells, $P = 0.0002$), and abnormal cristae (including distortion, stacking, or whirling) (Figure 7, A and B).

We further sought to investigate the mitochondrial function by measuring the respiration rate using Seahorse XF technology (Agilent), which allows concomitant analysis of the glycolysis rate. These analyses showed impaired mitochondrial respiration in ERCC1-deficient cells, which displayed a markedly lower basal oxygen consumption rate (OCR) than ERCC1-WT cells (Figure 7C). Conversely, the extracellular acidification rate (ECAR, an indicator of glycolysis) was markedly higher in the ERCC1-Hez and ERCC1-KO cells (Figure 7D). OCR under oligomycin (an inhibitor of ATP synthase), which measures respiration not producing ATP, was similar in all cell lines. This was also the case for the OCR under antimycin A (an inhibitor of respiratory complex III), which measures nonrespiratory oxygen consumption. In contrast, the maximal respiration rate under the maximal carbonyl cyanide 3-chlorophenylhydrazone (CCCP) dose appeared higher in ERCC1-WT and ERCC1-Hez than in ERCC1-KO cells, suggesting a higher respiratory complex content in the 2 former populations than in the latter one. As only 2 CCCP concentrations could be evaluated by Seahorse, we used high-resolution respirometry with the Oroboros O2k to extend CCCP titration. This complementary approach confirmed the decreased basal respiration and impaired maximal respiration in ERCC1-deficient populations (Supplemental Figure 8, A and B, all $P < 0.001$).

Because redox homeostasis is intimately tied to DNA repair and mitochondrial integrity, we assessed whether ROS were elevated in ERCC1-deficient cells, which could influence their response to

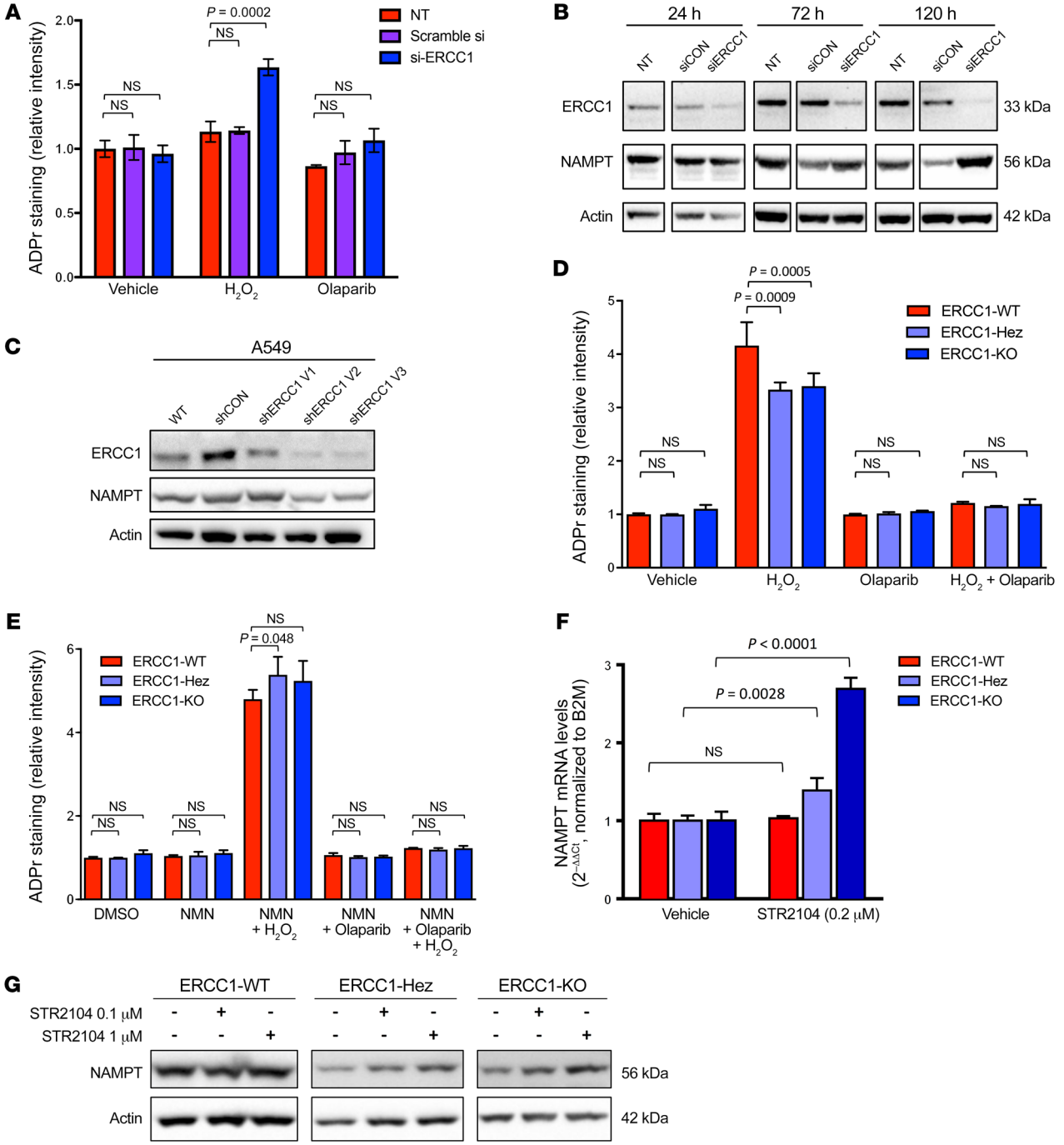

Figure 9. Loss of ERCC1 results in increased ADP-ribosylation and a gradual decrease in NAMPT expression. (**A**) ADP-ribosylation (ADPr) levels were measured by immunofluorescence in A549 cells not treated (NT) or treated with control (scramble siRNA) or ERCC1 siRNA (siERCC1). H_2O_2 exposure was used for inducing DNA damage. Olaparib was used as control for abrogation of PARP1-related ADP-ribosylation activity. Data are mean ADP-ribosylation activity ± SD from 1 of 3 independent experiments. (**B**) Representative Western blot of ERCC1 and NAMPT protein expression after acute ERCC1 silencing using siRNA in A549 cells. NT, nontransfected. Data were replicated in 2 independent experiments. (**C**) Western blot of ERCC1 and NAMPT protein expression after sequential transfections with shERCC1-coding viral particles in A549 cells. V1, V2, V3 indicate infections 1, 2, and 3, respectively, which were performed 10–15 days apart each. Data are from 1 experiment. (**D** and **E**) ADP-ribosylation levels were measured by immunofluorescence in the A549 isogenic model in the absence (**D**) or presence (**E**) of NMN supplementation. Data are mean ADP-ribosylation activity ± SD from 1 of 2 independent experiments. (**F**) Variations in NAMPT mRNA levels in A549 ERCC1-WT, ERCC1-Hez, and ERCC1-KO cell lines following 3-day exposure to nontoxic concentrations of the SIRT1 activator STR2104. Data represent mean $2^{-\Delta\Delta Ct}$ ± SD from 1 experiment. Statistical analyses are indicated (2-way ANOVA adjusted using Sidak's multiple comparison test). (**G**) Representative Western blot of NAMPT protein expression after 4-day exposure to nontoxic concentrations of STR2104. Data were replicated in 2 independent experiments. For **A**, **D**, **E**, statistical analyses are indicated (2-way ANOVA adjusted for multiple comparisons using Tukey's *t* test).

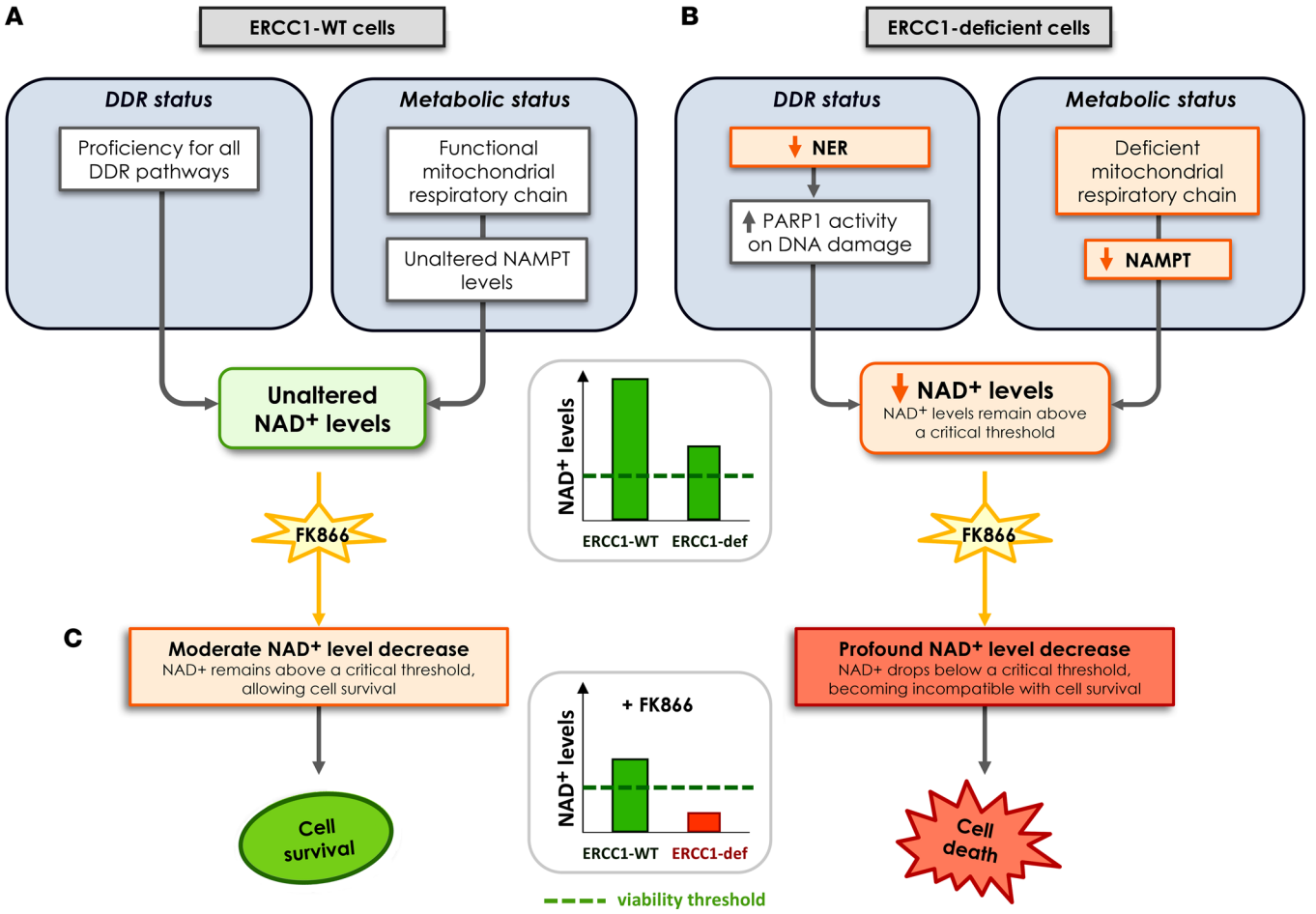

Figure 10. Proposed model for the synthetic lethality between NAMPT inhibition and ERCC1 deficiency in NSCLC cells. (**A**) ERCC1-proficient cells have a proficient DNA damage repair status and no metabolic alteration in the NAD^+ biosynthesis pathway. (**B**) Loss of ERCC1 induces decreased NER activity and dependency upon PARP1 activation for the repair of DNA lesions, thereby causing NAD^+ consumption. Chronic ERCC1 deficiency/PARP1 activation is associated with metabolic defects including decreased NAD^+ and NAMPT levels, as well as alterations in the mitochondrial respiratory chain. In this scenario, NAD^+ levels are low, but remain above a threshold that allows ERCC1-deficient cells to survive and proliferate. (**C**) Treatment with NAMPT inhibitors blocks the NAD^+ recycling pathway and causes an acute drop in NAD^+ levels. In ERCC1-proficient cells, NAD^+ levels remain above a critical threshold compatible with cell survival. In ERCC1-deficient cells, this acute drop in NAD^+ levels outstrips the cellular NAD^+ replenishment capacities and decompensates a fragile equilibrium; NAD^+ levels drop below a threshold compatible with cell survival, which triggers cell death. In this model, NAMPT and ERCC1 are synthetic lethal, as the combination of ERCC1 deficiency with NAMPT inhibition causes cell death, whereas each perturbation in isolation (i.e., ERCC1 deficiency or NAMPT inhibition) does not. Arrows represent a relationship and not a demonstrated causality link. DDR, DNA damage response; ERCC1-def, ERCC1-deficient; NER, nucleotide excision repair.

NAMPT inhibition. We used 6 complementary approaches which allowed us to evaluate: (a) intracellular ROS production (dihydroethidium), (b) extracellular ROS production (Amplex/HRP assay), (c) oxidative adducts (carbonyls and hydroxynonenal), and (d) the protein level of antioxidant enzymes (SOD1, SOD2, and PRDX3). All experiments indicated that ERCC1-deficient cells did not harbor any increased ROS levels (Supplemental Figure 9, A–G). Altogether, these results support that ERCC1 deficiency is associated with severe defects in mitochondrial structure and respiration in NSCLC models.

Loss of ERCC1 is associated with defects in mitochondrial respiratory chain complex IV. Because the SILAC screen originally identified a significant decrease in the expression of 3 subunits of the mitochondrial respiratory chain complex IV, we hypothesized that the respiratory defect observed in ERCC1-deficient cells might be related to defects in components of the mitochondrial electron transfer chain (ETC). We confirmed by Western blot the decrease of COX2 and COX4 subunits (Figure 8, A and B). Because protein expression of mitochondrial complexes is not necessarily correlated to activity, we further measured the enzymatic activity of complex IV using respiratory chain spectrophotometric assay (21). This showed a significant decrease in mitochondrial complex IV activity in ERCC1-KO cells (Figure 8C), which was rescued upon reintroduction of the functional ERCC1 isoform (Figure 8D). We used spectrophotometry to measure the enzymatic activities of mitochondrial complexes II, II+III, and citrate synthase activity; we did not find significant differences between ERCC1-proficient and ERCC1-deficient cells (Figure 8C). We further assessed the mitochondrial DNA (mtDNA) content in our A549 isogenic model using quantitative PCR. This showed a decrease in mtDNA copy number in ERCC1-KO populations, which was rescued upon reintroduction of the functional ERCC1 isoform (Supplemental Figure 10).

Sirtuin-1 (SIRT1) is an NAD^+-dependent nuclear deacetylase involved in the regulation of mitochondrial content (12, 22). Lower SIRT1 activity and altered mitochondrial metabolism or biogenesis have been associated with several pathological processes, including syndromes caused by defects in DNA repair proteins involved in NER (7). ERCC1-deficient cells displayed decreased SIRT1 expression on Western blot (Figure 8E). Although decreased SIRT1 expression may not confer decreased SIRT1 activity, this might suggest that the NAD^+/SIRT1 axis is downregulated in ERCC1-deficient cells, which would result in altered nuclear-mitochondrial signaling.

Acute ERCC1 defect causes increased ADP-ribosylation, whereas chronic ERCC1 defect is associated with reduced NAD^+ availability and decreased ADP-ribosylation capacities. Because ERCC1-deficient models had been chronically defective in ERCC1, we sought to evaluate the effects of the acute loss of ERCC1. ERCC1 silencing by siRNA was accompanied by increased ADP-ribosylation levels upon H_2O_2 exposure (Figure 9A), suggesting that PARP1 activation compensates for ERCC1 loss when DNA is damaged. Strikingly, we repeatedly observed an initial increase in NAMPT expression accompanying ERCC1 silencing, potentially indicating a cellular regulation loop aimed at maintaining the homeostasis of NAD^+ levels (Figure 9B). To mimic a progressive loss of ERCC1 over time, we performed several sequential cellular infections with viral particles encoding ERCC1 shRNA in the A549 cell line. This showed gradual loss of ERCC1 on repeated infections, which was associated with gradual decrease in NAMPT expression (Figure 9C). We went on to assess the DNA repair capabilities of ERCC1-deficient cells. As previously published (5), these cells do not have defects in RAD51 loading. We observed decreased ADP-ribosylation in the ERCC1-deficient isogenic models upon H_2O_2 exposure, which was rescued by the addition of NMN to the medium (Figure 9, D and E), suggesting that a low NAD^+ level limits PARP1 activation in cells with chronic ERCC1 deficiency.

We then sought to explore why NAMPT expression was, counterintuitively, decreased in ERCC1-deficient cells that present low NAD^+ levels. SIRT1 has previously been described as being able to regulate NAMPT levels (23). Because our previous experiments suggested decreased SIRT1 activity, we assessed the ability of STR2104, a SIRT1 activator, to restore NAMPT expression. Exposure to STR2104 at nonlethal concentrations allowed a dose-dependent increase of NAMPT expression both at the mRNA and protein levels, consistent with a regulation at the mRNA level (Figure 9, F and G). Collectively, these results suggest that NAD^+ levels are key in regulating the DNA damage response in ERCC1-deficient models.

A model for ERCC1-deficient NSCLC sensitivity to NAMPT inhibitors in which NAD^+ is the central sensor of fitness. One proposed model consistent with the data is shown in Figure 10. In this model, acute loss of ERCC1 induces dependency upon PARP1 activation for the repair of DNA lesions. Short-term PARP1 activation is beneficial for maintaining genomic stability, but results in a burst of NAD^+ consumption. In this scenario of transient and acute response, cellular responses to compensate for NAD^+ overconsumption are triggered, including NAMPT upregulation. This allows the NAD^+ level to be maintained. Chronic ERCC1 deficiency induces chronic PARP1 activation, which is eventually deleterious as it overcomes the cellular NAD^+ self-replenishment capacities. Chronic ERCC1 deficiency/PARP1 activation is associated with metabolic defects, including decreased NAD^+ and NAMPT levels, as well as alterations in the mitochondrial respiratory chain. In this scenario, NAD^+ levels are low, but remain above a critical threshold that allows ERCC1-deficient cells to survive and proliferate. Treatment with NAMPT inhibitors blocks the NAD^+ recycling pathway and causes an acute drop in NAD^+ levels. In ERCC1-proficient cells, NAD^+ levels remain above a critical threshold compatible with cell survival. In ERCC1-deficient cells, this acute drop in NAD^+ levels outstrips the cellular NAD^+ replenishment capacities and decompensates a fragile equilibrium: NAD^+ levels drop below a threshold compatible with cell survival, which triggers cell death. In this model, NAMPT and ERCC1 are synthetic lethal, as the combination of ERCC1 deficiency with NAMPT inhibition causes cell death, whereas each perturbation in isolation (i.e., ERCC1 deficiency or NAMPT inhibition) does not.

Discussion

Innovative approaches are urgently needed for NSCLC, which remains the leading cause of cancer death worldwide despite recent progress brought by targeted therapy and immune checkpoint blockers (1). Here, we report a link between ERCC1 deficiency and specific metabolic abnormalities (including a profound deficit in NAD^+ biosynthesis and mitochondrial defects), resulting in dramatic sensitivity to NAMPT inhibitors. Using a unique in-house–generated model of ERCC1 deficiency in NSCLC cell lines (4, 5, 13), we demonstrate that ERCC1-deficient populations are strikingly sensitive to NAMPT inhibitors in vitro and in vivo and that this exquisite sensitivity is a primary effect of ERCC1 deficiency. These findings represent an innovative therapeutic approach for NSCLC. Furthermore, we show that ERCC1-deficient populations display significant mitochondrial alterations, including ultrastructural abnormalities as well as an altered TCA cycle and respiratory defects. We propose a model where a decrease in NAMPT and NAD^+ links nuclear ERCC1 deficiency, mitochondrial defects, and associated metabolic abnormalities.

We believe that this is the first description of a synthetic lethal relationship between the nuclear DNA repair protein ERCC1 and energetic metabolism. Of note, the magnitude of the observed effect (1/1,000 therapeutic window in IC_{50} between ERCC1-WT and ERCC1-deficient cells) is similar to that observed with PARP inhibitors in BRCA-deficient populations (24), thereby opening promising therapeutic opportunities. Most importantly, the ERCC1-Hez cell line consistently behaved similarly to ERCC1-KO models, rather than similarly to ERCC1-proficient cells. This haploinsufficiency phenomenon was observed for NAMPT inhibitor sensitivity, metabolic profiling, and mitochondrial functions, but not for platinum sensitivity (Supplemental Figure 4, A and B). This is of tremendous importance for clinical applications because tumors often express low or minimal ERCC1 levels, which limits the efficacy of platinum salts and favors emergence of secondary resistance (4, 13). NAMPT inhibitors, either alone or in combination with drugs that show efficacy in ERCC1-deficient populations such as platinum salts or PARP inhibitors (5, 25), could therefore represent an interesting and innovative therapeutic approach.

Mitochondrial dysfunction is a common feature in cell degeneration and aging (22, 26). It has also been associated with diseases that result from DNA repair defects, in particular those associated with dysfunction of the NER proteins, including Cockayne syndrome and xeroderma pigmentosum. In humans, mutations in ERCC1 results in severe developmental defects at birth and premature death (27). Mouse models of ERCC1 deficiency display severe progeroid syndrome associated with progressive neurodegeneration, fat loss, and endocrine defects (28). To our knowledge, mitochondrial dysfunction has not been described so far in patients with ERCC1 deficiency. Our observations show that ERCC1 deficiency associates with alterations in mitochondrial metabolism and the NAD^+ recycling pathway in NSCLC models. Of note, our data were generated on a panel of tumor cell lines; it is possible that tumor-specific alterations such as *TP53* mutations, which have been shown to influence cellular metabolism, are present in some of them. The phenotype observed in our study may therefore be distinct in nontransformed primary cells. Interestingly, the association of NAD^+ depletion, decreased SIRT1 activity, and mitochondrial disturbances has recently been reported in several NER-deficient preclinical and patient-derived models — including CSA-, CSB-, XPA-, and XPD-deficient models (7–9) — as well as ATM-deficient models (11), where it has been linked to nucleus-to-mitochondria (NM) signaling. Decreased NAMPT and NAD^+ depletion (29–31), which may result in decreased SIRT1 activity (9, 32), loss of mitochondrial homeostasis, and hypersensitivity to NAMPT inhibitors (33), have also been reported in circumstances of increased genotoxic stress. To our knowledge, it has not yet been reported in ERCC1 defects in vivo nor in ERCC1-deficient cancer cells. We therefore believe that our findings are novel, but are in line with several previous observations in noncancerous models with alternative NER defects.

Although all our observations are consistent with the proposed model (Figure 10) and with previous literature data derived from other DNA repair deficiencies (7–9, 11), alternative mechanistic explanations might be considered. Redox homeostasis is intimately linked to DNA repair and increased ROS might have rendered cells more sensitive to NAMPT inhibitors. However, we did not observe elevated ROS levels in ERCC1-deficient cells (Supplemental Figure 9). A role for ERCC1 in the repair of mtDNA lesions and maintenance of mtDNA genome integrity could also be hypothesized, even though NER is traditionally the only DNA repair pathway absent from mammalian mitochondria (34). Whether ERCC1 is involved in the resolution of specific structures during mtDNA replication or decatenation might also warrant further investigation. Moreover, reliable assessment of ERCC1 functionality in tumors has been proven to be challenging, notably because of the presence of several closely related isoforms, thus precluding efficient distinction between ERCC1 isoforms with the currently available technologies (4). In that context, integrating a metabolic or mitochondrial hallmark as an additional surrogate biomarker of ERCC1 functionality, alongside the evaluation of ERCC1 expression, might be considered. The significant correlation observed on our series of 55 lung adenocarcinoma cases between ERCC1 and NAMPT IHC staining reinforces this hypothesis.

ERCC1 plays a key role in stabilizing XPF and enhancing its endonuclease activity. Although the heterodimer is a key player of the NER pathway (35, 36), it also has additional roles in the interstrand crosslink repair and double-strand break repair pathways (37, 38). As most ERCC1 functions have been linked to XPF endonuclease activity, which has also been reported as a biomarker in some tumor types (37, 38), the conclusions from this work might be applicable to XPF-deficient malignancies as well. Recent studies reported that ERCC1 also possesses XPF-independent functions (39, 40). The persistence of normal XPF levels and cisplatin resistance in the ERCC1-Hez cell lines (4, 5, 13) contrasted with the significant NAMPT decrease and NAMPT small-molecule inhibitor sensitivity observed in this latter population. Complete ERCC1 deficiency is thought to be embryonic lethal in humans, and only 3 ERCC1-deficient patients have been described so far (27, 41). This contrasts with the higher frequency of patients suffering from NER-associated disorders, and highlights that ERCC1 deficiency in humans leads to a much more severe phenotype (27). Whether these metabolic deficiencies result from an XPF-independent function of ERCC1 might be hypothesized (39, 40).

There is growing interest in exploiting metabolic defects and mitochondrial dysfunction to selectively induce cancer cell death. In this context, several novel NAMPT inhibitors are currently being developed (e.g., OT-82, LSN3154567, and KPT-9274). FK866 (APO866) has been proven tolerable at active doses in a phase 1 trial, although dose escalation was limited by thrombocytopenia (16). Our findings indicate that ERCC1-deficient tumors may respond to NAMPT inhibitors at lower doses than their ERCC1-proficient counterparts, which may enable reaching antitumor activity while avoiding excessive toxicities in selected populations thanks to a favorable therapeutic window. In addition, by analogy with the folate rescue used for high-dose methotrexate administration, whether the tolerability of these drugs might be improved by adding sequential vitamin B3 or NMN administration (14, 19) might deserve clinical evaluation. Similarly, alternative schedules that use more frequent administration at lower doses might be worth exploring in order to achieve similar drug exposure and avoid peak-related, dose-limiting toxicity. In this context, clinical trials currently evaluating NAMPT inhibitors may benefit from dedicated designs that would associate a dose-escalation phase exploring several schedules of administration, and potentially including a vitamin B3–based rescue, with a dose-expansion phase in appropriately molecularly selected patients, including patients with ERCC1-deficient malignancies.

In summary, we have demonstrated a synthetic lethal relationship between ERCC1 deficiency and NAMPT inhibition in NSCLC models. These findings represent promising therapeutic opportunities that exploit a nucleus-to-mitochondria crosstalk. Considering the current development of several NAMPT inhibitors, we hope that these findings will rapidly translate into clinical evaluation through early-phase trials performed in appropriately molecularly selected populations.

Methods

Cell lines. WT A549 and H1975 cells were purchased from the American Type Culture Collection (ATCC). A549/H1975 ERCC1-deficient cells (ERCC1-Hez, ERCC1-KO1, and ERCC1-KO2) and rescue clones (ERCC1-KO, KO + isof 201, KO + isof 202, KO + isof 203, KO + isof 204) were generated as described previously (13). Cell lines were

grown in DMEM (A549) or RPMI (H1975) (Gibco) supplemented with 10% FBS in a humidified atmosphere of 5% CO_2 at 37°C. All cell lines were tested for the absence of mycoplasma.

Viability assays. For short-term viability assays, cells were plated in 96-well plates and treated the following day for 5 days. Cell viability was assessed using the luminescent CellTiter-Glo reagent (Promega) according to the manufacturer's protocol. Luminescence was measured using the Victor X4 Multilabel Plate Reader (PerkinElmer). Dose-response curves and IC_{50} were generated using Prism 6 (GraphPad Software) after log transformation of the data. Curves were extrapolated using nonlinear regression with 4-parameter logistic regression fitting on triplicates from survival fractions of at least 3 replicates, following the model: y = Bottom + (Top – Bottom)/(1 + $10^{([LogIC50 - x] \times HillSlope)}$). For colony formation survival assay, cells were seeded in 6-well plates at 500–1,500 cells/well and treated the following day. Drug- or vehicle-containing media was replenished twice weekly for 10–14 days. Cells were fixed and stained with 0.5% crystal violet solution in 25% methanol. Viability was assessed by colony counting. For both short-term viability assays and colony formation survival assay, the surviving fraction (SF) for each X concentration was calculated as SF = mean viability in treated sample at concentration X/mean viability of untreated samples (vehicle).

Antibodies. ERCC1 (catalog FL-297) and HSC70 (catalog B-6) antibodies were purchased from Santa Cruz. NAMPT (catalog 14A.5) antibody was purchased from EMD Millipore. SIRT1 (catalog 19A7AB4), COX4 (catalog 20E8C12), PRDX3 (catalog EPR8115), and HSP60 (catalog ab46798) antibodies were purchased from Abcam. β-Actin (catalog A1978), SOD1 (catalog HPA001401), SOD2 (catalog HPA001814), DHE (catalog D7008), and β-tubulin (catalog T8328-100UL) antibodies were purchased from Sigma-Aldrich. Anti-COX2 and -HNE antibodies were kindly provided by Anne Lombès (Institut Cochin, Paris, France) and were previously described (42, 43). DNP (2,4-dinitrophenyl) hydrazone derivatives were measured using the OxyBlot Protein Oxidation Detection Kit S7150 (EMD Millipore).

Stable isotope labeling by amino acids in cell culture (SILAC). Cells were grown in SILAC DMEM supplemented with either isotope-labeled (Lys 8, Arg 10) or unlabeled amino acids for 8 doubling times. Peptides were extracted as described in the Supplemental Material and Methods section. Reversed-phase chromatography was performed using an HP1200 platform (Agilent). Mass spectrometry was performed on a LTQ Velos Orbitrap mass spectrometer (ThermoFisher Scientific). Data analysis was performed as indicated in the Supplemental Methods.

Metabolomic profiling. Cells were seeded in 6-well plates in DMEM supplemented with 10% FBS; vehicle or FK866 was added when they reached 80% of confluence and an exponential growth phase. After 24 hours of vehicle/drug exposure, cells were rinsed for 2 seconds with cold milliQ-grade water, and were lysed by scrapping in 500 μl cold methanol/water (9:1, v/v, –20°C) containing internal standards. Lysates of 2 replicates were combined in microcentrifuge tubes and cold chloroform (100 μl, –20°C) was added before vortexing for 30 seconds and final centrifugation at 12,500 *g* for 10 minutes at 4°C. Supernatant was collected and evaporated using a pneumatically assisted concentrator (Techne DB3) at 40°C. On the day of chemical analysis, 300 μl methanol was added to the dried extract and the solution was equally split for GC-MS/MS analysis and LC-MS/MS + LC-QTOF analyses. Metabolomics protocols were run as described previously (44). Reversal of flow to succinate from fumarate was addressed using succinate, fumarate, and methylmalonic acid measurements by GC-MS/MS after 24 hours of treatment with vehicle or the succinate dehydrogenase inhibitor methylmalonic acid (2 mM, a dose which did not impact cell growth or survival in vitro), as described in ref. 45. Further details on metabolic analysis are provided in Supplemental Material and Methods.

Transmission electron microscopy. One million cells were fixed in 2% glutaraldehyde in 0.1 M phosphate buffer for 1 hour at 4°C, collected by scraping, centrifuged, and postfixed in 2% osmium tetroxide. Following ethanol dehydration, cell pellets were embedded in Epon 812 (Electron Microscopy Sciences). Ultrathin sections were stained with standard uranyl acetate and lead citrate prior to observation with a Tecnai 12 electron microscope (FEI, ThermoFisher Scientific). Digital images were taken with a SISMegaviewIII charge-coupled device camera (Olympus).

Subcutaneous xenografts and drug treatment. Two million A549 ERCC1-WT or ERCC1-KO cells were injected s.c. in the flanks of 6-week-old athymic nude (nu/nu) mice (n = 8 mice per group; Charles River Laboratories). Mice carrying 100-mm^3 subcutaneous tumors were randomized to receive 30 mg/kg/day FK866 (Sigma-Aldrich) or vehicle (30% PEG, 5% Tween 80, dextrose 5% in water) by i.p. injection twice daily, 4 days on, 3 days off, for 6 weeks. Tumor diameters were measured by the same experienced technician with digital caliper, and tumor volumes were estimated using the formula: 0.5 × length × $width^2$. Body weights were monitored twice weekly.

siRNA and shRNA. For siRNA experiments, WT cells were reverse-transfected with Lipofectamine RNA iMAX (Life Technologies) as indicated by the manufacturer, using nontargeting siRNA (D-001206-13-05, Dharmacon), siERCC1 (LU-006311-00-0002, GE Healthcare), and siNAMT (M-004581-01, Dharmacon). For shRNA experiments, HEK293T cells were transfected with lentiviral plasmids encoding ERCC1 shRNA (pLOK.1, REF RHS4533-EG2067) and packaging vectors (pCMV-R8.74 and pMD2G, http://www.addgene.org/) in order to produce lentiviral particles. After harvesting and concentration of lentiviral particles, A549 cells were infected with shERCC1-encoding particles by adding lentiviral particles in the culture media. Puromycin was added after 48 hours, in order to select infected clones. Three cycles of infection were realized in A549 cells each 10–15 days apart, followed by puromycin selection.

ADP-ribosylation. Levels of ADP-ribosylation were measured by indirect immunofluorescence as described in ref. 46. Cells were incubated overnight with drug-free media, 1 μM olaparib, and/or 100 μM NMN. Olaparib, a PARP1/2 inhibitor that blocks DNA PARylation reactions, was used as a negative control. Cells were subsequently exposed to 1 mM H_2O_2 for 10 minutes and fixed with ice-cold methanol. ADP-ribose levels were quantified by high-throughput imaging (Operetta, PerkinElmer), using the anti-pan–ADP-ribose binding reagent (H10 monoclonal antibody 4335-AMC-050, Trevigen). The nuclear ADP-ribose levels of treated cells were plotted versus the levels measured in untreated cells.

Study approval. All in vivo studies were approved by the local ethical committee of University Paris-Sud no. 26 (authorized project 2012-083).

Statistics. The number of samples, experimental repeats, and details on statistical tests are indicated in the relevant figure legends. Adjusted P values were calculated using Prism 6, GraphPad Software, and were considered significant when $P < 0.05$. For metabolomics analyses, difference in metabolites were considered significant when the false discovery rate (FDR) was less than 0.1.

Where applicable, the means of population averages from multiple independent experiments (± SD or SEM) are indicated. The in vivo experiments were randomized. No samples or animals were omitted from data analyses.

Author contributions

MT performed and analyzed in vivo mouse studies, short-term viability and long-term colony formation assays, oxygen consumption and extracellular acidification rate studies, mitochondrial complexes activity studies, intracellular and extracellular ROS production measurements, and gene and protein expression studies. ND performed and analyzed in vivo mouse studies, extracellular ROS production measurements, short-term viability assays, siRNA and shRNA silencing experiments, gene and protein expression studies, and supported metabolomics and transmission electronic microscopy experiments. MG performed and analyzed short-term viability assays, siRNA and shRNA silencing experiments, and gene and protein expression studies. DM performed and analyzed gene and protein expression studies. RMC performed and analyzed study of the cell death mechanism. DBK and JF performed and analyzed study of ADP-ribosylation. LB performed and analyzed in vivo mouse studies. JA performed and analyzed tissue immunohistochemistry studies. SD performed metabolomics experiments; SD and CP analyzed and interpreted the data. AL performed and analyzed oxygen consumption and extracellular acidification rate studies, mitochondrial complexes activity studies, intracellular ROS production measurements, and oxidative adducts and antioxidant enzymes studies. S. Souquere and GP performed and analyzed transmission electronic microscopy experiments. FM and SPV performed and analyzed stable isotope labeling by amino acids in cell culture experiments. TS, S. Sauvaigo, MSK, AS, KAO, LF, FB, AA, AL, CJL, and JCS supported design of the study and analysis of the data. AL, CJL, JCS, and AA contributed to writing the manuscript. JCS acquired funding for the study and supervised the Thorax U981 group. MT and SPV designed the study, supervised the project, analyzed and interpreted the data, and wrote the manuscript. All authors discussed the results and commented on the manuscript.

Acknowledgments

MT received financial support from ITMO Cancer AVIESAN (Alliance Nationale pour les Sciences de la Vie et de la Santé, National Alliance for Life Sciences & Health) within the framework of the Cancer Plan 2014–2019. The Thorax U981 group (MT, TS, ND, RMC, MG, DM, MSK, KAO, LF, JCS, and SPV) was supported by the Etablissement Public Chancellerie des Universités de Paris (Legs Poix), the Fondation de France (Engt 2013 00038309), the Fondation ARC pour la Recherche sur le Cancer (PJA 20131200170), Agence National de la Recherche (ANR-10-IHBU-0001), and SIRIC SOCRATE funded by Institut National du Cancer (INCa-DGOS-INSERM6043). The Gene Function Team (Institute of Cancer Research) was funded by Cancer Research UK (grant C347/A8363), Breast Cancer Now, and The EU FP7 project EurocanPlatform (grant 260791). The authors thank David Enot (Gustave Roussy, Université Paris-Saclay) for the analysis and interpretation of all metabolomics experiments; Chris Ottolenghi (Hôpital Necker-Enfants Malades, Assistance Publique-Hôpitaux de Paris, Paris Descartes University) and Miria Ricchetti (Institut Pasteur) who provided insight and expertise that greatly assisted the research; Corinne Dupuy (Gustave Roussy, Inserm, Université Paris-Saclay) for advice and comments in analyzing ROS production; Caroline L'Hermitte-Stead (Institut Cochin, Paris Descartes University) for assistance with ROS, oxidative adducts, and antioxidant enzyme studies; Melanie Collet (Gustave Roussy, Université Paris-Saclay) for technical assistance for immunohistochemical analyses; and Fabrice André (Gustave Roussy, Université Paris-Saclay) for having welcomed MT in his laboratory.

Address correspondence to: Sophie Postel-Vinay or Jean-Charles Soria, Drug Development Department, Gustave Roussy, 114 rue Edouard Vaillant, Villejuif 94805, France. Phone: 33.1.42.11.43.43; Email: sophie.postel-vinay@gustaveroussy.fr (S. Postel-Vinay). Phone: 33.1.42.11.42.96; Email: jean-charles.soria@gustaveroussy.fr (J.-C. Soria).

1. Global Burden of Disease Cancer Collaboration, et al. Global, regional, and national cancer incidence, mortality, years of life lost, years lived with disability, and disability-adjusted life-years for 32 cancer groups, 1990 to 2015: a systematic analysis for the global burden of disease study. *JAMA Oncol*. 2017;3(4):524–548.
2. Postel-Vinay S, Vanhecke E, Olaussen KA, Lord CJ, Ashworth A, Soria JC. The potential of exploiting DNA-repair defects for optimizing lung cancer treatment. *Nat Rev Clin Oncol*. 2012;9(3):144–155.
3. Olaussen KA, et al. DNA repair by ERCC1 in non-small-cell lung cancer and cisplatin-based adjuvant chemotherapy. *N Engl J Med*. 2006;355(10):983–991.
4. Friboulet L, et al. ERCC1 isoform expression and DNA repair in non-small-cell lung cancer. *N Engl J Med*. 2013;368(12):1101–1110.
5. Postel-Vinay S, et al. A high-throughput screen identifies PARP1/2 inhibitors as a potential therapy for ERCC1-deficient non-small cell lung cancer. *Oncogene*. 2013;32(47):5377–5387.
6. Lord CJ, Ashworth A. PARP inhibitors: Synthetic lethality in the clinic. *Science*. 2017;355(6330):1152–1158.
7. Fang EF, Scheibye-Knudsen M, Chua KF, Mattson MP, Croteau DL, Bohr VA. Nuclear DNA damage signalling to mitochondria in ageing. *Nat Rev Mol Cell Biol*. 2016;17(5):308–321.
8. Fang EF, et al. Defective mitophagy in XPA via PARP-1 hyperactivation and NAD(+)/SIRT1 reduction. *Cell*. 2014;157(4):882–896.
9. Scheibye-Knudsen M, et al. A high-fat diet and NAD(+) activate Sirt1 to rescue premature aging in Cockayne syndrome. *Cell Metab*. 2014;20(5):840–855.
10. Chatre L, Biard DS, Sarasin A, Ricchetti M. Reversal of mitochondrial defects with CSB-dependent serine protease inhibitors in patient cells of the progeroid Cockayne syndrome. *Proc Natl Acad Sci U S A*. 2015;112(22):E2910–E2919.
11. Croteau DL, Fang EF, Nilsen H, Bohr VA. NAD+ in DNA repair and mitochondrial maintenance. *Cell Cycle*. 2017;16(6):491–492.
12. Cantó C, Menzies KJ, Auwerx J. NAD(+) metabolism and the control of energy homeostasis: a balancing act between mitochondria and the nucleus. *Cell Metab*. 2015;22(1):31–53.
13. Friboulet L, et al. ERCC1 function in nuclear excision and interstrand crosslink repair pathways is mediated exclusively by the ERCC1-202 isoform. *Cell Cycle*. 2013;12(20):3298–3306.
14. Chiarugi A, Dölle C, Felici R, Ziegler M. The NAD metabolome--a key determinant of cancer cell biology. *Nat Rev Cancer*. 2012;12(11):741–752.
15. Kim MY, Zhang T, Kraus WL. Poly(ADP-ribosyl)ation by PARP-1: 'PAR-laying' NAD+ into a nuclear signal. *Genes Dev*. 2005;19(17):1951–1967.
16. Holen K, Saltz LB, Hollywood E, Burk K, Hanauske AR. The pharmacokinetics, toxicities, and biologic effects of FK866, a nicotinamide adenine dinucleotide biosynthesis inhibitor. *Invest New Drugs*. 2008;26(1):45–51.
17. Zhao G, et al. Discovery of a highly selective NAMPT inhibitor that demonstrates robust efficacy and improved retinal toxicity with nicotinic acid coadministration. *Mol Cancer Ther*. 2017;16(12):2677–2688.
18. Barretina J, et al. The Cancer Cell Line Encyclo-

pedia enables predictive modelling of anticancer drug sensitivity. *Nature*. 2012;483(7391):603–607.
19. Olesen UH, Thougaard AV, Jensen PB, Sehested M. A preclinical study on the rescue of normal tissue by nicotinic acid in high-dose treatment with APO866, a specific nicotinamide phosphoribosyltransferase inhibitor. *Mol Cancer Ther*. 2010;9(6):1609–1617.
20. Wallace DC. Mitochondrial diseases in man and mouse. *Science*. 1999;283(5407):1482–1488.
21. Medja F, et al. Development and implementation of standardized respiratory chain spectrophotometric assays for clinical diagnosis. *Mitochondrion*. 2009;9(5):331–339.
22. Gomes AP, et al. Declining NAD(+) induces a pseudohypoxic state disrupting nuclear-mitochondrial communication during aging. *Cell*. 2013;155(7):1624–1638.
23. Verdin E. NAD^+ in aging, metabolism, and neurodegeneration. *Science*. 2015;350(6265):1208–1213.
24. Farmer H, et al. Targeting the DNA repair defect in BRCA mutant cells as a therapeutic strategy. *Nature*. 2005;434(7035):917–921.
25. Bajrami I, et al. Synthetic lethality of PARP and NAMPT inhibition in triple-negative breast cancer cells. *EMBO Mol Med*. 2012;4(10):1087–1096.
26. Hoeijmakers JH. DNA damage, aging, and cancer. *N Engl J Med*. 2009;361(15):1475–1485.
27. Jaspers NG, et al. First reported patient with human ERCC1 deficiency has cerebro-oculo-facio-skeletal syndrome with a mild defect in nucleotide excision repair and severe developmental failure. *Am J Hum Genet*. 2007;80(3):457–466.
28. Niedernhofer LJ, et al. A new progeroid syndrome reveals that genotoxic stress suppresses the somatotroph axis. *Nature*. 2006;444(7122):1038–1043.
29. Tang JB, et al. Bioenergetic metabolites regulate base excision repair-dependent cell death in response to DNA damage. *Mol Cancer Res*. 2010;8(1):67–79.
30. Alano CC, Garnier P, Ying W, Higashi Y, Kauppinen TM, Swanson RA. NAD+ depletion is necessary and sufficient for poly(ADP-ribose) polymerase-1-mediated neuronal death. *J Neurosci*. 2010;30(8):2967–2978.
31. Wang G, et al. P7C3 neuroprotective chemicals function by activating the rate-limiting enzyme in NAD salvage. *Cell*. 2014;158(6):1324–1334.
32. Bai P, et al. PARP-1 inhibition increases mitochondrial metabolism through SIRT1 activation. *Cell Metab*. 2011;13(4):461–468.
33. Chan M, et al. Synergy between the NAMPT inhibitor GMX1777(8) and pemetrexed in non-small cell lung cancer cells is mediated by PARP activation and enhanced NAD consumption. *Cancer Res*. 2014;74(21):5948–5954.
34. Kazak L, Reyes A, Holt IJ. Minimizing the damage: repair pathways keep mitochondrial DNA intact. *Nat Rev Mol Cell Biol*. 2012;13(10):659–671.
35. Fagbemi AF, Orelli B, Schärer OD. Regulation of endonuclease activity in human nucleotide excision repair. *DNA Repair (Amst)*. 2011;10(7):722–729.
36. Schärer OD. Nucleotide excision repair in eukaryotes. *Cold Spring Harb Perspect Biol*. 2013;5(10):a012609.
37. Kirschner K, Melton DW. Multiple roles of the ERCC1-XPF endonuclease in DNA repair and resistance to anticancer drugs. *Anticancer Res*. 2010;30(9):3223–3232.
38. McNeil EM, Melton DW. DNA repair endonuclease ERCC1-XPF as a novel therapeutic target to overcome chemoresistance in cancer therapy. *Nucleic Acids Res*. 2012;40(20):9990–10004.
39. Rageul J, Frëmin C, Ezan F, Baffet G, Langouët S. The knock-down of ERCC1 but not of XPF causes multinucleation. *DNA Repair (Amst)*. 2011;10(9):978–990.
40. Yang L, Ritchie AM, Melton DW. Disruption of DNA repair in cancer cells by ubiquitination of a destabilising dimerization domain of nucleotide excision repair protein ERCC1. *Oncotarget*. 2017;8(33):55246–55264.
41. Kashiyama K, et al. Malfunction of nuclease ERCC1-XPF results in diverse clinical manifestations and causes Cockayne syndrome, xeroderma pigmentosum, and Fanconi anemia. *Am J Hum Genet*. 2013;92(5):807–819.
42. Barthélémy C, et al. Late-onset mitochondrial DNA depletion: DNA copy number, multiple deletions, and compensation. *Ann Neurol*. 2001;49(5):607–617.
43. Ahmed EK, Rogowska-Wrzesinska A, Roepstorff P, Bulteau AL, Friguet B. Protein modification and replicative senescence of WI-38 human embryonic fibroblasts. *Aging Cell*. 2010;9(2):252–272.
44. Enot DP, et al. Metabolomic analyses reveal that anti-aging metabolites are depleted by palmitate but increased by oleate in vivo. *Cell Cycle*. 2015;14(15):2399–2407.
45. Chouchani ET, et al. Ischaemic accumulation of succinate controls reperfusion injury through mitochondrial ROS. *Nature*. 2014;515(7527):431–435.
46. Hoch NC, et al. XRCC1 mutation is associated with PARP1 hyperactivation and cerebellar ataxia. *Nature*. 2017;541(7635):87–91.